Billiard balls and matter-wave interferometry

R. Friedberg
Department of Physics, Barnard College, Columbia University, New York, New York 10027

S. R. Hartmann
Department of Physics, Columbia University, New York, New York 10027
(Received 21 May 1992; revised manuscript received 25 November 1992)

The billiard-ball model (BBM) is redeveloped to allow quantitative diagrammatic evaluation of signal parameters associated with optical coherent transient experiments. It is expanded to include the action of external forces and fields as well as to include atomic-beam-type experiments. Matter-wave interferometric experiments are examined in the context of the BBM and their relationship to photon-echo experiments is explored.

PACS number(s): 42.50.Md, 07.60.Ly, 42.50.Vk

I. INTRODUCTION

The billiard-ball model [1] (BBM) of the interaction of freely moving atoms (or molecules) with pulsed radiation has been introduced as a method of visualization alternative to the better known vector model [2] which is more appropriate for self-induced transparency [3] and photon echoes in a solid [4]. It leads to a quick prescription for locating delayed coherences (echoes) by observing crossings of lines (trajectories) in a *recoil diagram* [1].

The present paper has a fourfold purpose: to present a detailed prescription analogous to Feynman rules for calculating the strength of echo signals; to demonstrate that this prescription is founded on an analysis as thorough as any commonly used in the literature for these experiments; to show how the whole scheme can be carried over to atomic-beam experiments in the Ramsey-fringe category; and to extend the prescription by one additional rule which makes it applicable to matter-wave interferometry.

Recently, matter-wave interferometry has been used in a gas for the potentially precise measurement of the acceleration of gravity [5] and in an atomic beam as a sensitive detector of rotational motion [6]. Prior work has concentrated on splitting or reflecting matter waves coherently. The methods used have incorporated a transmission grating [7], a double slit [8], a superfluid coated mirror [9], and a standing light wave [10]. The common thread weaving through these experiments is the controlled modification of atomic trajectories in order to achieve a desired interference.

The related area of physics that deals with optical coherent transients in gases is conventionally analyzed in a manner which masks the intimate connection with the aforementioned experiments since the Doppler effect is treated formally as a frequency shift and the actual atomic recoil trajectories do not appear in the analysis. This connection is more nearly suggested by the billiard-ball model [1] which represents echoes in gases as a consequence of an interference between two atomic trajectories.

We propose therefore to illuminate the connection between the recent matter-wave experiments and the optical coherent transient experiments that have preceded them by expanding the BBM to include the effects of external forces and fields. In the process of this expansion we will develop a more thorough theoretical foundation for the billiard-ball model and facilitate its use by deriving "Feynman rules" which allow the diagrams to yield quantitative expressions for signal amplitudes. We will also extend its application to the analysis of Ramsey fringe and related experiments [11] as well as to coherent-scattering experiments [12]. We shall find that the BBM is especially well suited for their analysis and that experiments performed in the past have a more direct bearing on present day work than is commonly appreciated.

The billiard-ball model, like many models in physics, consists of three components: (1) a way to picture a physical process; (2) a way to predict observations on the basis of the entities pictured; (3) an argument or derivation that justifies these predictions.

The picture in this model is of atoms or molecules as objects of a definite extent (not the physical diameter of a real atom but that of an artificially constructed wave packet) which respond classically to the impulse of optical absorption and emission and to external forces. In the spirit of the Feynman path integral, one habitually compares two classical trajectories corresponding to different absorption and emission histories. Thus one imagines a pair of "billiard balls," initially superimposed, separating and perhaps reencountering one another in the course of time.

The predictions have to do with interference effects between two of these trajectories. There are two kinds of predictions.

(a) The first kind is qualitative predictions which tell when such an effect exists. The model asserts that two trajectories interfere when the two billiard balls overlap in space. If the respective trajectories correspond to optical histories, one of which leaves the atom excited and the other not, the interference may produce coherent emission (an echo). If both histories leave the atom in the

same state, the interference contributes a term to population inversion which is usually made manifest by contriving to make the relative phase of the two trajectories depend on a variable parameter under external control (thus producing "fringes").

The spatial crossing of trajectories is easily visualized with the aid of "recoil diagrams," which are essentially graphs of displacement versus time, except that only that part of the displacement is shown which results from photonic impulses, since the rest is common to the two trajectories. Thus the segments between short optical pulses are always straight lines in the diagram.

(b) The second kind is quantitative predictions which tell how strong the signal is. In this paper we explain in general how to calculate signal strength by multiplying together various factors derived from the parts of the recoil diagram. There are factors of magnitude derived from the atomic dipole moment and pulse strength at each "vertex" of the diagram (see Rule 1, Sec. II D), and from the degree of overlap of the two billiard balls at the observation time (see Rule 6; this factor is temperature dependent in a gas and represents the effect of Doppler dephasing). There are also phase factors associated with each vertex (Rule 2) and with each line segment (Rule 3) of the diagram. In addition, there may be a phase factor (Rule 4) associated with the whole diagram and determined by the graphical "area" (dimension =distance×time) between the two trajectories as shown on the diagram. This factor gives the effect of external forces due to gravity or rotation and has not been previously discussed in terms of the BBM.

The argument justifying a model may be based on a literal assertion of the physical picture's approximate truth, as in deriving the equation of state from the molecular picture of an ideal gas. Or it may be based on an appeal to a truer (i.e., better established) if less conceptually accessible theory, which is proved under certain conditions or approximations to yield the same answers as the model, as in justifying the classical action formula for quantum tunneling by developing the WKB approximation of the Schrödinger equation. The billiard-ball model follows rather the second pattern.

In particular, the model has two features which are not necessarily asserted to be literally true but are justified by an argument that they lead to the same conclusions as the truth. First, we neglect the diffractive spreading of the wave packet in time. The fact that this does not affect the answer is more clearly *seen* in momentum space [see (3.45)–(3.51)] but can be usefully *applied* in position space as a justification for the "substitute wave function" which gives the billiard ball an unchanging diameter.

Second, we choose the initial wave packet to be as narrow in space as possible (this determines the billiard-ball size) without being inconsistent with the Doppler-broadened width of the resonance line. That is, we let the atomic wave function be a quantum superposition of all the momenta that enter into the Maxwell-Boltzmann distribution. We show that this is equivalent, with respect to the outcome of the experiments we consider, to the reasonable assertion that the momentum distribution of each wave packet is uncorrelated with the location of its center of mass.

Both of these issues are better understood by considering the density matrix ρ of an atom in the momentum basis. If the resonance line really has a sharp homogeneous width then $\rho_{\mathbf{q}\mathbf{q}'}$ must essentially vanish unless the momenta $\hbar\mathbf{q}$, $\hbar\mathbf{q}'$ are very close. On the other hand, $\rho_{\mathbf{q}\mathbf{q}}$ receives support from the whole Maxwell-Boltzmann distribution. In attributing to the atom a compact wave packet with the same momentum support as $\rho_{\mathbf{q}\mathbf{q}}$, we are simply giving the off-diagonal elements nonzero values instead of the correct vanishing ones; in neglecting diffractive spreading we are fixing these artificial values in time instead of allowing them to oscillate in accordance with the Schrödinger equation. The justification in both cases comes down to the claim that the off-diagonal elements will cancel out anyway in calculating the signal, because of the sum over many atoms homogeneously distributed in position.

The foregoing discussion applies most directly to a gas; to apply it to an atomic beam one should keep in mind mainly transverse momenta. The longitudinal extent of the wave packet is more appropriately dealt with by an additional argument given in Appendix B.

Throughout this paper we shall assume that the sample is optically thin and that the excitation pulses are short compared to the inverse linewidth. The pulses are resonant within a margin of error inverse to the pulse *length,* but not necessarily so within a measure of length inverse to the pulse *separation.* Although it is usually a simple matter to include relaxation in the *BB* calculation we have omitted relaxation factors entirely in the present paper because their inclusion requires a more sophisticated justification.

We begin in Sec. II with a reconciliation, on a very qualitative level, of an apparent intuitive contradiction between the billiard-ball (BB) picture of Doppler dephasing and the picture based on thermal velocities. We then treat some simple cases illustrating the use of recoil diagrams to locate coherences, extending their use to Ramsey fringe experiments as well as to interferometry. We then provide the Feynman-like rules which make them applicable to quantitative calculations yielding the strength of the coherent signal. All of Sec. II is merely prescriptive: it shows how to use recoil diagrams to get answers.

In Sec. III we give a general derivation (for arbitrary pulse schemes) of the rules asserted in Sec. II. In Sec. IV we consider specific matter-wave interferometric experiments including one performed earlier in this laboratory but not so classified at the time.

II. BILLIARD-BALL FUNDAMENTALS

A. Wave packets and trajectories

The purpose of the BBM is to provide a heuristic yet theoretically correct framework in which to describe coherent optical transient phenomena in gases. It accomplishes this by expressing the action of coherent laser excitation pulses, single or multiphoton resonant with the gaseous elements, in a manner which leads to an exact

and obvious interpretation. Each excitation pulse induces optical transitions promoting the gaseous elements (atoms or molecules) into superposition states. This results in the representation of each such state as a collection of wave packets associated with various internal histories. Expectation values of induced radiative moments or state populations involve the overlap integral between two such wave packets.

Although the individual wave packets undergo a complicated diffractive spreading in the course of time, it is found [see (3.51) below, also [1]] that *this spreading has no effect on the overlap integral.* It thus suffices to follow the unspread wave packet (billiard ball) as it divides and recoils in response to the action of laser fields. The overlapping of the various billiard balls signals the presence of coherences which manifest themselves as free radiation decays, photon echoes, generalized echoes, Ramsey fringes, etc., as the case may be. We follow the billiard-ball trajectories by constructing recoil diagrams. As we shall see, these recoil diagrams are simply constructed and unaffected by the presence of other external forces and fields. The effect of the latter is simply to introduce an overall phase factor.

The idea behind the BBM is thus to represent an atom or molecule by a wave packet which is initially located at $\mathbf{r}=\mathbf{R}_s$,

$$\psi_s(\mathbf{r},t=0)=F(\mathbf{r}-\mathbf{R}_s,0) \tag{2.1}$$

and then follow its development in time as it is subjected to external forces and fields. In general the effect of each excitation pulse is to generate additional wave packets representing the new states coupled to by the pulse. (The full wave function is a sum of such packets each multiplied by the corresponding intrinsic state ket.) Following one of these wave packets, which we label p, we write its development as

$$\psi_{s,p}(\mathbf{r},t)=e^{i(\mathbf{K}_p\cdot\mathbf{r}-\Phi_p)}F(\mathbf{r}-\mathbf{r}'-\mathbf{r}_p''-\mathbf{R}_s,t)\ , \tag{2.2}$$

where $\mathbf{r}''$ is the displacement due to recoil from laser fields and $\mathbf{r}'$ is the displacement due to the action of gravity, rotations, external fields, etc. Here $\mathbf{K}_p$ is the net momentum received by the billiard ball from photons up to time t and Φ_p is a phase which depends on the action, up to time t, of the external forces and fields present. The time appears explicitly as a separate argument to indicate wave-packet spreading. It is implicitly included in both $\mathbf{r}'$ and $\mathbf{r}''$.

When the time comes to evaluate optical coherences it is found that it suffices to replace the true wave packet (2.2) with a substitute wave packet

$$\hat{\Psi}_{s,p}(\mathbf{r},t)=e^{i(\mathbf{K}_p\cdot\mathbf{r}-\hat{\Phi}_p)}F(\mathbf{r}-\mathbf{r}_p''-\mathbf{R}_s,0)\ . \tag{2.3}$$

This means that diffractive spreading can be ignored and along with it the dependence of the wave-packet motion on the displacement $\mathbf{r}'$. The effect of $\mathbf{r}'$ is felt only in the modified phase factor $\hat{\Phi}_p$. [In both (2.2) and (2.3) we have omitted a constant prefactor: see (3.46) and (3.51).]

B. Free-radiation decay: dephasing time

The simplest application of the BBM is in the calculation of the free-radiation decay (the analog of free-induction decay in magnetic resonance) following resonant excitation of an optical transition by a short laser pulse. Immediately after excitation by a pulse with wave vector $\mathbf{k}$ a macroscopic polarization density is generated which is also characterized by $\mathbf{k}$. This ordered array radiates into $\mathbf{k}$ until random atomic motion degrades the order and the radiated field associated with it.

1. Standard argument

The standard analysis would correctly argue that the time constant associated with this decay is the Doppler dephasing time T_{Doppler}. It is just the time that an atom moving at a typical thermal velocity, $\mathbf{v}_{\text{thermal}}\approx\sqrt{3k_BT/m}$, where T is the temperature and k_B is the Boltzmann factor, takes to move an optical wavelength λ_{optical}

$$\mathbf{v}_{\text{thermal}}T_{\text{Doppler}}=\lambda_{\text{optical}}\ . \tag{2.4}$$

2. Billiard-ball argument

The BB analysis would argue that one should use the time T_{recoil} it takes for the excited-state wave packet, recoiling (with velocity $\mathbf{v}_{\text{recoil}}$) after being generated by a photon with momentum $\hbar\mathbf{k}$, to displace itself from the stationary ground-state wave packet. Since the size of each atomic wave packet is the thermal deBroglie wavelength $\lambda_{\text{deBroglie}}$, we have

$$\mathbf{v}_{\text{recoil}}T_{\text{recoil}}=\lambda_{\text{deBroglie}}\ . \tag{2.5}$$

3. Reconciliation

The terms in (2.4) and (2.5) are related by the momentum conservation condition

$$m\,\mathbf{v}_{\text{recoil}}h/\lambda_{\text{optical}} \tag{2.6}$$

and the momentum spread which determines the wave-packet size

$$m\,\mathbf{v}_{\text{thermal}}=h/\lambda_{\text{deBroglie}}\ . \tag{2.7}$$

Combining all of the above we have

$$T_{\text{recoil}}=T_{\text{Doppler}}\ , \tag{2.8}$$

showing that the conventional and BB analyses yield identical results.

4. Comment

The equivalence of these two approaches is sometimes surprising since for a gas at room temperature $\mathbf{v}_{\text{thermal}}\gg\mathbf{v}_{\text{recoil}}$. The surprise is allayed, however, when it is realized that this inequality is compensated by $\lambda_{\text{deBroglie}}\ll\lambda_{\text{optical}}$. In estimating the angular diffraction of light through an aperture one can either (1) consider light as a wave and use Huygens's principle or (2) use the

uncertainty principle while treating light as composed of particles (photons). For this problem, as for the free-radiation decay problem, neither method has a clearcut advantage. For more complicated problems, such as those involving photon-echo generation, the billiard-ball method has several clearly superior features.

We note that the equivalence of these two calculations does not *require* that $\lambda_{\text{deBroglie}} \ll \lambda_{\text{optical}}$, and nowhere in the paper do we make this assumption. The fact that $\lambda_{\text{deBroglie}}$ and λ_{optical} have the same dimension is an accident: their quotient has no importance, and nothing special happens when $\lambda_{\text{deBroglie}} \approx \lambda_{\text{optical}}$. Hence the billiard-ball model is just as applicable to a cold gas in which $\lambda_{\text{deBroglie}} \geq \lambda_{\text{optical}}$ as to a strongly Doppler-broadened one.

C. Recoil diagrams

BB analysis is facilitated by the construction of recoil diagrams [1] which show the wave-packet trajectories responding to the action of the laser-pulse fields alone. Note that only $\mathbf{r}''$, not $\mathbf{r}'$, appears in (2.3). In the interval between laser excitation pulses the recoil momentum $m\dot{\mathbf{r}}''$ of each wave packet is constant in time. Thus these trajectories are always simple segmented straight lines even when external fields (gravitational, rotational, etc.) are applied. Each such line is a graph showing the temporal evolution of $\mathbf{r}''$ in (2.3); its slope is proportional to $\mathbf{K}_p$ in (2.3). The whole "substitute wave function" contains a term for each trajectory. The central rule is that whenever trajectories cross or superimpose coherences occur [1]. As we shall see, the effect of any external field is to introduce an overall phase factor onto the wave packet and for a uniform field this phase is simply proportional to the graphical area under the recoil trajectory.

1. Momentum conservation

The phase-matching condition in a gas is supplemented by the constraint that the recoil diagram must *close* (two trajectories must intersect) with a tolerance $\lambda_{\text{deBroglie}}$ = billiard-ball diameter. [Otherwise the functions F in (2.3) would not overlap.] This imposes a relationship among the wave vectors and it follows that not all excitation schemes that respect phase matching will produce a coherent signal.

2. Free-radiation decay

The simplest recoil diagram is that associated with the action of a single optical pulse, cf. Fig. 1. The trajectory crossing is at t_1. As the excited-state trajectory recedes from that of the ground state, the wave-packet overlap diminishes as does the coherently radiated field. In the figure we show the overlap at two successive times, first at a time when there is small overlap and then later when the overlap is gone.

The wave packets (billiard balls) have been shown perforce as extending (meaninglessly) along the t axis, but the component of the width shown as horizontal really has nothing to do with any time interval and represents the extent of the balls in the spatial direction transverse to the pulse propagation direction. We have depicted the balls as spherical

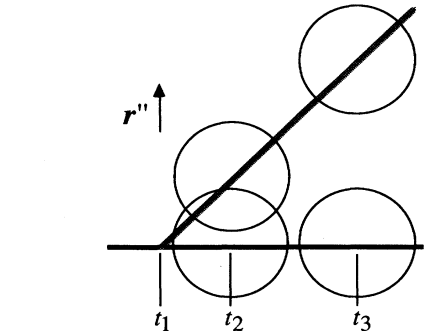

FIG. 1. Recoil ($\mathbf{r}''$ vs t) diagram for free-radiation decay. The recoil displacement $\mathbf{r}''(t)$ is drawn vs t. Ground-state trajectory is solid, excited-state shaded. Billiard balls are represented by circles. Laser pulse is applied at t_1. As long as the circles overlap we may regard this diagram as "closed" in an extended sense.

implying that the optical pulse has a wide bandwidth. When the optical pulse has a narrow bandwidth only those atoms whose velocity along $\mathbf{k}$ (taken here to be in the vertical, ↑, direction) is in a sufficiently restricted range will be excited and the excited wave packets therefore becomes elongated, i.e., ellipsoidal

as shown here [13,14]. Replacing the spherical wave packets in Fig. 1 with the elliptical ones increases the interval over which the overlap persists and thereby reduces the Doppler dephasing.

3. Ramsey fringes

The next recoil diagram of simple character is that describing the excited-state trajectories of atoms subjected to two successive copropagating optical pulses, cf. Fig. 2. Here the wave-packet overlap in the excited state does not diminish in time. This overlap yields an interference term in the excited-state population which oscillates as a function of excitation laser frequency. (See "Discussion of Rule 2", Sec. II D 3) Because the excited-state trajectories are parallel the interference term is independent of when it is detected. If the second excitation pulse is delayed further, the second excited-state trajectory will be displaced to the right and the wave-packet overlap will be diminished. Thus the Ramsey signal is diminished in the same manner as the free-radiation decay, i.e., it is subject to Doppler dephasing.

In an atomic beam the difference in t_2 and t_1 is just $t_2 - t_1 = \mathbf{v}_{\parallel}^{-1} D$, where $\mathbf{v}_{\parallel}$ is the atomic velocity along the beam and D is the distance between the laser excitation beams. The vertical direction in Fig. 2 is then transverse to the atomic beam since in all cases we take the former to be parallel to the laser beams.

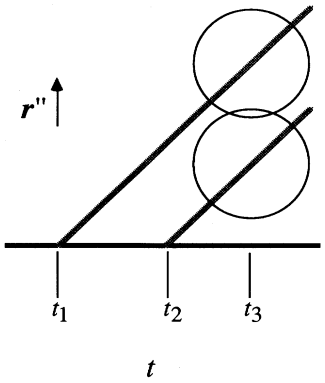

FIG. 2. Recoil ($\mathbf{r}''$ vs t) diagram for Ramsey fringes. Laser pulses applied at t_1 and t_2. Billiard-ball overlap, shown at t_3, is independent of t. Overlap decreases as t_2-t_1 increases, signifying Doppler dephasing.

4. Photon echoes

The application of a second excitation pulse not only produces a second excited-state trajectory such as shown in Fig. 2 but a second ground-state trajectory, cf. Fig. 3. This is the complete recoil diagram for two-pulse excitation. The subsequent crossing of the ground- and excited-state trajectories gives rise to the photon echo. This crossing, in the BBM, corresponds to the elimination of Doppler dephasing.

5. Recoil displacement as a vector

In viewing these diagrams, the reader is asked for some tolerance for the fact that the recoil diagrams should really be drawn on four-dimensional paper in order to display the three components of $\mathbf{r}''$ as well as one of t. On two-dimensional paper we have to be content with the component of $\mathbf{r}''$ in a direction approximately parallel to all the $\mathbf{k}_j$; of course it can be chosen exactly parallel to all $\mathbf{k}_j$ if the pulses are strictly colinear. Then $\mathbf{r}''$ has no transverse component. It is customary, however, in many echo experiments to angle the two pulses slightly so that the echo will not be masked by pulse afterimage. In that case the two trajectories p_1 and p_2 of Fig. 3, drawn properly on four-dimensional paper, would fail to cross by a distance $(\hbar/m)|\mathbf{k}_1-\mathbf{k}_2|\tau$ in the transverse direction. When this distance becomes comparable to the transverse diameter of the billiard ball the echo intensity falls off. Measurement of this effect has been used to determine the billiard-ball shape [14].

6. Doppler-free Ramsey fringes

Doppler dephasing can also be eliminated from the Ramsey-fringe experiment (Fig. 2) by using two pulses to produce a crossing of trajectories at which a third pulse sets up a population interference. The original scheme [15] involves three pulses equally spaced in time: the first pulse propagates forward, the last backward, and the middle pulse is a standing wave. The resulting recoil diagram is given in Fig. 4(a). [The accompanying "excitation diagram" Fig. 4(b) will be explained in Sec. II E.] Only the essential trajectories are shown. The excited-state trajectory shown following the second pulse is directed downward because one photon has been stimulated in the direction of the initial pulse and one photon (coming from the opposite direction) has been absorbed. After the third pulse the two excited-state trajectories are not only parallel but coincident. This coincidence reflects the absence of Doppler dephasing of the excited-state population signal, regardless of the length of τ.

From the foregoing exposition, the reader familiar with echo experiments might wonder why it would not serve as well to send all three pulses in the forward direction, obtaining the recoil diagram of Fig. 5. Again the population interference is set up at a crossing so that the subsequent excited-state trajectories coincide.

The answer is that although the scheme of Fig. 5 will

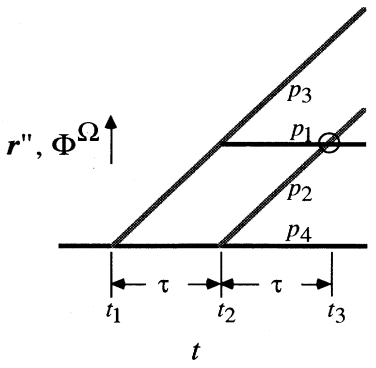

FIG. 3. Recoil ($\mathbf{r}''$ vs t) and excitation (Φ^Ω vs t) diagrams for photon echo. Copropagating laser pulses applied at t_1 and $t_2=t_1+\tau$. The excitation diagram is explained in Sec. II E. Thus the crossing at $t_3=t_2+\tau$ allows echo formation in both solids and gases. The separate trajectories are labeled p_1, p_2, p_3, and p_4.

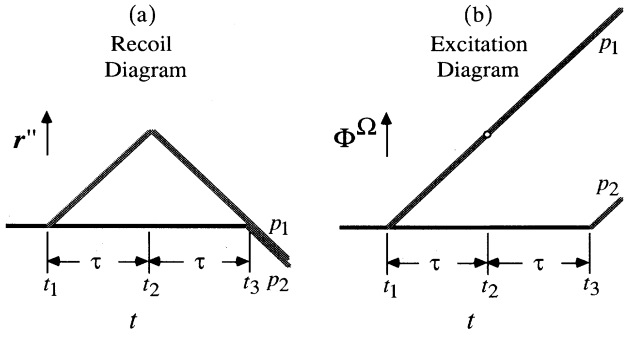

FIG. 4. (a) Recoil ($\mathbf{r}''$ vs t) and (b) excitation (Φ^Ω vs t) diagrams for Ramsey fringes. First of two contributions (see Fig. 7). The first and third pulse propagate oppositely, the second pulse is a standing wave. Here diagrams are distinct. (a) shows the coherent excited-state superposition forming at t_3 in a gas or atomic beam. Nonclosure of (b) means that this coherence will display Ramsey fringes but that echoes will not form in a solid. [See Sec. II E for an explanation of (b)].

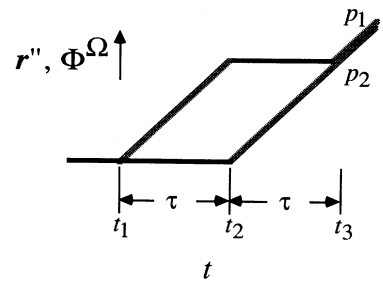

FIG. 5. Recoil ($\mathbf{r}''$ vs t) and excitation (Φ^{Ω} vs t) diagrams for the gravity experiment. Equally spaced (by τ) copropagating laser pulses applied at t_1, t_2, and t_3. Coherent excited-state superposition forms at t_3. Ramsey fringes are forbidden if only one laser is used but allowed when several are used (cf. Sec. II E). Gravity induces a phase shift proportional to the enclosed area in the recoil diagram.

produce a Doppler-free *population* interference, it will not produce *fringes* because detuning the laser will not change the phase relation between the two trajectories, whereas it will do so in Fig. 4. This distinction can be graphically understood by shifting one's attention from the recoil diagram to the accompanying "excitation diagram" which will be explained in Sec. II E. It is possible, however, to obtain fringes in Fig. 5 by detuning the three pulses by different amounts, as was done in the "gravity experiment" [5] which will be discussed in Sec. IV D.

On the other hand, the scheme of Fig. 4, without the third pulse, can be used to create echoes in a gas but not in a solid. This will be explained in Sec. II E.

7. *Interferometry*

A feature of the recoil diagrams not heretofore discussed is that they directly display the phase interference which results from the action of gravity, rotation, external fields, etc. Associated with any coherence exposed by the crossing of two trajectories is the graphical area $\mathbf{A}=\int(\mathbf{r}_p''-\mathbf{r}_{p'}'')dt$ that these two trajectories enclose. The beauty of the recoil diagrams is that this phase interference is just $\Phi^{1}=(m/\hbar)\dot{\mathbf{v}}\cdot\mathbf{A}$ when the acceleration $\dot{\mathbf{v}}$ of the atoms, due to the action of gravity, etc., is constant in time. (The effect of the radiation pulses is not included in $\dot{\mathbf{v}}$.) This coefficient $\dot{\mathbf{v}}$ is not pictorially represented in the recoil diagram, which shows only the atomic recoil caused by the emission or absorption of photons from the exciting laser beams. Thus the action of gravity, etc. does not complicate the geometry of the recoil diagrams as it is not (and should not be) incorporated into them. Only the graphical area $\mathbf{A}$, which multiplies $\dot{\mathbf{v}}$, is to be read from the diagram.

The dimension of $\mathbf{A}$ is distance $\times$ time, and it is therefore not a true area [16]. Nevertheless, in atomic-beam experiments it is closely related to the geometrical area between trajectories which in simple cases is $|\mathbf{v}_{\parallel}\mathbf{A}|$ in our notation, $\mathbf{v}_{\parallel}$ being the atomic velocity along the beam. Note, though, that $\mathbf{A}$ carries the vector character of $\mathbf{r}''$, not of $\mathbf{r}''\times\mathbf{v}_{\parallel}$. For experiments in a thermal vapor $\mathbf{A}$ has no corresponding geometrical area.

D. Diagrammatic rules

The recoil diagrams' primary function is to show by way of their geometry when and under what conditions coherences occur and interferometric phase terms arise. They also serve as "Feynman diagrams" which, according to simple rules, allow for speedy evaluation of wavefunction amplitudes and expectation values.

1. *Rules: traveling-wave excitation*

Consider any recoil diagram resulting from the application of a series of pulses and isolate one trajectory. Label it p for path. If a pulse connects the present electronic state to another we say it generates a vertex. We shall call this vertex "active" if the atom on path p actually changes its state, "inactive" if it does not. (An inactive vertex generates a factor reducing the amplitude.) Let the jth vertex occur at t_j and the electronic energy just following the vertex be $\hbar\Omega_{jp}$.

We treat first the case where the pulse is a traveling wave, $\mathrm{Re}e^{i(\mathbf{k}_j\cdot\mathbf{r}-\omega_j t-\varphi_j)}$ where $\omega_j=k_j c$. Then we have the following.

Rule 1. To each vertex we associate an amplitude B_{jp} which depends on the amplitude, duration, and character of the excitation pulse, and on whether the vertex is active or inactive. For a traveling-wave pulse of area θ_j

$$B_{jp}=\begin{cases} i\sin\dfrac{\theta_j}{2} & \text{if the vertex is active} \\ \cos\dfrac{\theta_j}{2} & \text{if the vertex is inactive .} \end{cases}$$

Rule 2. To each vertex we associate a phase

$$\Phi_{jp}^{\varphi}=\begin{cases} \pm\mathbf{k}_j\cdot\mathbf{r}-\Phi_{jp}^{\omega} & \text{if the vertex is active .} \\ 0 & \text{if the vertex is inactive ,} \end{cases}$$

where $\Phi_{jp}^{\omega}=\pm(\omega_j t_j+\varphi_j)$. The ambiguous sign is $+$ if a photon is absorbed, $-$ if emitted.

Rule 3. To the interval between the successive active vertices j and j' we associate the phase

$$\Phi_{jp}^{\epsilon}=\Phi_{jp}^{\Omega}+\Phi_{jp}^{K^2}=-\left[\Omega_{jp}+\frac{\hbar}{2m}\mathbf{K}_{jp}^2\right](t_{j'}-t_j)\ ,$$

unless the jth is the last active vertex in which case $t_{j'}\to t$. [The cumulative recoil momentum $\mathbf{K}_{jp}$ is defined after (2.2).]

Rule 4. When the atoms are acted on by spatially uniform and time-independent external forces (gravity, Coriolis, etc.) then in addition to the above there is an overall phase

$$\Phi_p^{\iota}=-\frac{m}{\hbar}\dot{\mathbf{v}}t\cdot\mathbf{r}_p''(t)+\frac{m}{\hbar}\dot{\mathbf{v}}\cdot\mathbf{A}_p\ , \tag{2.9}$$

where $\mathbf{A}_p$ is the graphical area under the trajectory of

path p. We have assumed that $\dot{\mathbf{v}}$ is constant, and t is measured from an origin before the first pulse. This rule is derived, see (3.55), from a more general formula (3.41) which applies to variable forces as well.

Rule 5. The above amplitudes and phases combine to yield the wave-packet amplitude

$$u_p = \left[\prod_j B_{jp}\right] \exp\left[i\left[\sum_j \Phi^{\varphi}_{jp} + \sum_j \Phi^{\epsilon}_{jp} + \Phi^{\iota}_p\right]\right]$$
$$= \left[\prod_j B_{jp}\right] e^{i(\mathbf{K}_p\cdot\mathbf{r}-\Phi_p)} ,$$

where

$$\Phi_p = \sum_j \Phi^{\omega}_{jp} - \sum_j \Phi^{\epsilon}_{jp} - \Phi^{\iota}_p$$

and j runs over the vertices. The prefactor $\prod_j B_{jp}$ was omitted in (2.3). See below, (3.13), for an explicit definition of $\mathbf{K}_p$.

The remaining rules apply to expressing the signal observables $\langle\langle \mathbf{P} e^{-i\mathbf{k}\cdot\mathbf{r}}_{n_1 n_2} \rangle\rangle$ and $\langle\langle N_n \rangle\rangle$, where the inner bracket denotes a quantum matrix element and the outer an integral over the position of the atom. (The N atoms contained in the sample are assumed to be distributed over a region of linear dimension large compared to an optical wavelength.) Thus $\langle\langle \mathbf{P} e^{-i\mathbf{k}\cdot\mathbf{r}}_{n_1 n_2} \rangle\rangle$ is the dipole emission source for the transition $|n_1\rangle \rightarrow |n_2\rangle$ [see (3.22)], and $\langle\langle N_n \rangle\rangle$, the population in state $|n\rangle$.

Suppose that the system is to be observed at a time t. Any coherent signal will be indicated by a pair of trajectories p_1, p_2 that cross or nearly cross at time t.

Rule 6. If the two trajectories are separated at time t by a spatial distance $\Delta\mathbf{r}'' = \Delta\mathbf{r}''(t) = \mathbf{r}''_{p_1} - \mathbf{r}''_{p_2}$ then the signal will depend on the *billiard-ball overlap factor* defined by

$$f_{p_1 p_2}(t) = e^{-(mk_B T/2\hbar^2)(\Delta\mathbf{r}'')^2} ,$$

where T is the temperature and k_B is Boltzmann's constant. This rule shows the sensitivity to trajectory crossing.

Rule 7. Once the quantities u_p for all p and $f_{p_1 p_2}$ for all p_1, p_2 have been found then for any pair of final states $|n_1\rangle, |n_2\rangle$ we define the coherence product

$$U_{n_1 n_2} = (2\pi)^3 N \sum_{p_1}^{n_1} \sum_{p_2}^{n_2} u_{p_1} u^*_{p_2} f_{p_1 p_2}(t) ,$$

where $\sum_p^n$ denotes the sum over all trajectories p that terminate in $|n\rangle$. We note that the combination

$$U_{n_1 n_2} = (2\pi)^3 N u_{p_1} u^*_{p_2} f_{p_1 p_2}(t)$$

is obtained from the $M_{p_1 p_2}(\mathbf{k})$ of (3.32) after some manipulation: see (3.52).

Rule 8. Measured signals are related to $U_{n_1 n_2}$ as follows: the population in the state $|n\rangle$ is given by

$$\langle\langle N_n \rangle\rangle = U_{nn}$$

and the source determining emission along $\mathbf{k}$ from $n_1 \rightarrow n_2$ is given by

$$\langle\langle \mathbf{P} e^{-i\mathbf{k}\cdot\mathbf{r}}_{n_1 n_2} \rangle\rangle = \mathbf{p}_{n_1 n_2} U_{n_1 n_2} .$$

Here $\mathbf{p}_{n_1 n_2} = \langle n_2 | \mathbf{P} | n_1 \rangle$.

Purely for reference in reading the rest of the paper, we give here a list of the various phases Φ, without the attendant subscripts, defined above.

Rule 2,

$$\Phi^{\omega} = \pm(\omega t + \varphi) ,$$

$$\Phi^{\varphi} = \pm\mathbf{k}\cdot\mathbf{r} - \Phi^{\omega} = \pm(\mathbf{k}\cdot\mathbf{r} - \omega t - \varphi) .$$

Rule 3,

$$\Phi^{\Omega} = -\Omega\Delta t ,$$

$$\Phi^{K^2} = -\frac{\hbar}{2m} K^2 \Delta t ,$$

$$\Phi^{\epsilon} = \Phi^{\Omega} + \Phi^{K^2} = -\left[\frac{\hbar}{2m} K^2 + \Omega\right]\Delta t .$$

Rule 4,

$$\Phi^{\iota} = \frac{m}{\hbar}(-\dot{\mathbf{v}} t\cdot\mathbf{r}'' + \dot{\mathbf{v}}\cdot\mathbf{A}) .$$

Rule 5,

$$\Phi = \sum(\Phi^{\omega} - \Phi^{\epsilon}) - \Phi^{\iota} ,$$

$$\mathbf{K}\cdot\mathbf{r} - \Phi = \sum(\Phi^{\varphi} + \Phi^{\epsilon}) + \Phi^{\iota} .$$

2. *Rules: standing-wave excitation*

It is sometimes necessary to apply standing-wave rather than traveling-wave pulses. The effect is to produce a fanlike array of trajectories as any number of photons $\hbar\mathbf{k}_j$ can be absorbed and emitted (cf. Fig. 6). The total momentum transferred to the atom will be $m\hbar\mathbf{k}$, where

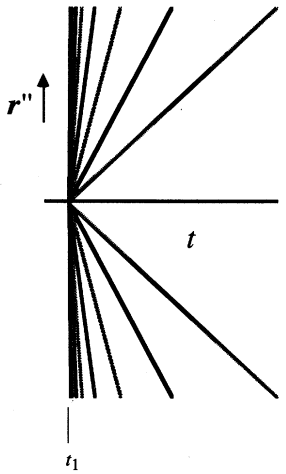

FIG. 6. Recoil ($\mathbf{r}''$ vs t) diagram for free-radiation decay and standing-wave excitation. The laser pulse is applied at t_1 which produces a physical grating and a free-radiation decay along $\pm\mathbf{k}_j$.

m ranges over all integers from $-\infty$ to $+\infty$. For the sake of generality we describe the jth standing-wave pulse as two traveling-wave pulses $\mathrm{Re}e^{i(\mathbf{k}_j\cdot\mathbf{r}-\omega_j t-\varphi_j^+)}$ $+\mathrm{Re}e^{i(-\mathbf{k}_j\cdot\mathbf{r}-\omega_j t-\varphi_j^-)}$.

The rules in this case are like those for the traveling wave except that the first two are changed to the following.

Rule (1'). For a standing-wave pulse of area θ_j at the crest, the amplitude associated with a vertex is given by a Bessel function $B_{jp}=J_m(\theta_j/2)$, where the vertex is active for odd m and inactive for even m.

Rule (2'). To each vertex we associate a phase

$$\Phi_{jp}^{\varphi}=m\left[\mathbf{k}\cdot\mathbf{r}-\frac{\varphi_j^+-\varphi_j^-}{2}\right]-\eta_{jp}\left[\omega_j t_j+\frac{\varphi_j^++\varphi_j^-}{2}\right]$$

where

$$\eta_{jp}\begin{cases}=0 & \text{if } m \text{ is even}\\ =\pm 1 & \text{if } m \text{ is odd},\end{cases}$$

the ambiguous sign being the same as in rule 2.

With the above modified rules we are able to retain Rules 3–6 with no further change. Any mix of traveling- and standing-wave pulses is now covered.

3. *Discussion of rules*

Closed diagrams—simplification of Rule 4. Coherences occur when recoil trajectories cross, i.e., diagrams close. But when they do, then $\mathbf{r}_p''(t)$, evaluated at the crossing, is the same for both paths and the term $(m/\hbar)\dot{\mathbf{v}}t\cdot\mathbf{r}_p''(t)$ drops out so that the phase difference becomes

$$\Delta\Phi^{\iota}=\Phi_p^{\iota}-\Phi_{p'}^{\iota}=(m/\hbar)\dot{\mathbf{v}}\cdot\mathbf{A}\ , \tag{2.10}$$

where $\mathbf{A}=\mathbf{A}_p-\mathbf{A}_{p'}$ is the enclosed area. This phase is the basis of interferometric experiments as it depends on the atomic motion ($m\dot{\mathbf{v}}=\mathbf{F}_{\text{external}}=\text{const}$) responding to the action of external forces or fields.

Discussion of Rule 1. The coefficients B_{jp} are necessary in obtaining the magnitude of the coherences. This is especially important in cases when multiple coherences must be added together. For the Doppler-free Ramsey fringes of Fig. 4 there is another relevant diagram, cf. Fig. 7. The interference between the diagrams of Figs. 4 and Fig. 7 is constructive and the coherence is reinforced.

Discussion of Rule 2. The phase associated with each vertex includes the phase of the exciting laser fields and is responsible for the amplitude modulations obtained on varying the laser tuning, i.e., Ramsey fringes. For the diagrams of Fig. 4,

$$\Phi_{p_1}^{\varphi}=+(\mathbf{k}_+\cdot\mathbf{r}-\omega t_1-\varphi_1)-(\mathbf{k}_+\cdot\mathbf{r}-\omega t_2-\varphi_2)+(\mathbf{k}_-\cdot\mathbf{r}-\omega t_2-\varphi_2')$$

and

$$\Phi_{p_2}^{\varphi}=+(\mathbf{k}_-\cdot\mathbf{r}-\omega t_3-\varphi_3)$$

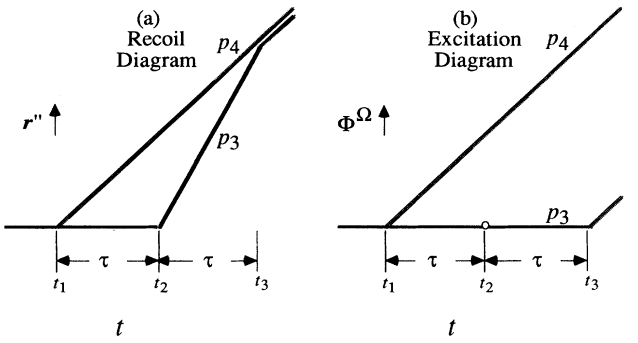

FIG. 7. (a) Recoil ($\mathbf{r}''$ vs t) and (b) excitation (Φ^{Ω} vs t) diagrams for Doppler-free Ramsey fringes. The second of the two contributions to Ramsey-fringe production. See Fig. 5 caption. The steeply sloping segment of p_3 after the second pulse represents the ground state, and so the vertex of p_3 at t_2 is inactive.

where the fields are counterpropagating, i.e., $\mathbf{k}_+=-\mathbf{k}_-$. Thus

$$\begin{aligned}\Delta\Phi_{p_1p_2}^{\varphi}&=\Phi_{p_1}^{\varphi}-\Phi_{p_2}^{\varphi}\\&=\omega(t_3-t_1)+(\varphi_3-\varphi_1+\varphi_2-\varphi_2')\\&=2\omega\tau+(\varphi_3-\varphi_1+\varphi_2-\varphi_2')\end{aligned}$$

and as long as the laser is coherent (so that the phase differences are constant) Ramsey fringes result from the dependence on ω. The coefficient 2τ gives the inverse spacing of the fringes. [The phases φ_1, φ_2 (φ_2'), and φ_3 refer, respectively, to the first pulse, forward (backward) component of the second pulse, and third pulse.]

If we had gone to the photon echo configuration and applied a third pulse at t_3 we would generate an excited-state coherence which would not exhibit Ramsey fringes, cf. Fig. 5. The analysis follows the above; here copropagating traveling waves are used and

$$\Phi_{p_1}^{\varphi}=+(\mathbf{k}_+\cdot\mathbf{r}-\omega t_1-\varphi_1)-(\mathbf{k}_+\cdot\mathbf{r}-\omega t_2-\varphi_2)+(\mathbf{k}_+\cdot\mathbf{r}-\omega t_3-\varphi_3)$$

and

$$\Phi_{p_2}^{\varphi}=+(\mathbf{k}_+\cdot\mathbf{r}-\omega t_2-\varphi_2)$$

to obtain

$$\begin{aligned}\Delta\Phi_{p_1p_2}^{\varphi}&=\omega(t_3-2t_2+t_1)+(\varphi_1-2\varphi_2+\varphi_3)\\&=(\varphi_1-2\varphi_2+\varphi_3)\ ,\end{aligned}$$

which is independent of ω.

Discussion of Rule 3. The overall phase associated with the electronic states is

$$\Phi_p^{\epsilon}=-\int_0^t\left[\Omega_p+\frac{\hbar}{2m}\mathbf{K}_p^2\right]dt'\ , \tag{2.11}$$

where $\Omega_p=\Omega_p(t)$ is the eigenfrequency associated with the electronic state on trajectory (path) p at any

time t and $(\hbar^2/2m)\mathbf{K}_p^2$ is the recoil energy. One might expect additional kinetic terms such as $(\hbar/2m)\mathbf{Q}^2, (\hbar/2m)2\mathbf{Q}\cdot\mathbf{K}_p$, where $\hbar\mathbf{Q}$ is the atomic momentum without recoil; but these either cancel or are represented in Rule 4 (see Sec. III C).

It is best to separate the contributions in Ω_p from those in $(\hbar^2/2m)\mathbf{K}_p^2$. We write

$$\Phi_p^{K^2} = \sum_j^{t_j<t} \Phi_{jp}^{k^2} = -\frac{\hbar}{2m}\int_0^t \mathbf{K}_p^2 dt' \tag{2.12}$$

for the quadratic recoil phase and

$$\Phi_p^{\Omega} = \sum_j^{t_j<t} \Phi_{jp}^{\Omega} = -\int_0^t \Omega_p dt' \tag{2.13}$$

for the excitation phase.

When multiple interfering coherences occur, $\Delta\Phi_{pp'}^{K^2}$ (where $\Delta\Phi_{pp'}\equiv\Phi_p-\Phi_{p'}$) can vary independently of $\Delta\Phi_{pp'}^{\varphi}$ according to the particular p, p' combination. A simple example is the interfering Ramsey-fringe coherences depicted in Figs. 4 and 7. Application of Rules 2 and 3 in this case yields

$$\Delta\Phi_{pp'}^{\varphi}+\Delta\Phi_{pp'}^{K^2} = 2\omega\tau+(\varphi_3-\varphi_1+\varphi_2-\varphi_2') \pm\frac{\hbar}{2m}(2k^2\tau)\ ,$$

where we use $(-)$ for $p=p_1$, $p'=p_2$ in Fig. 4, and $(+)$ for $p=p_4$, $p'=p_3$ in Fig. 7. The quadratic recoil correction, which shifts the fringes arising from each diagram, is small, but with increasing sensitivity possible it should not be neglected. In this case it weakens the constructive interference between the two diagrams.

The contribution from Φ_p^{Ω} is another matter. In a gas or atomic beam the quantum-mechanical frequency Ω_p has a single value as has $\Phi_p^{\Omega}(t)$. In a solid the Ω_p's are spread out and give rise to inhomogeneous broadening. The behavior of $\Phi_p^{\Omega}(t)$ thus determines the coherences in a solid just as the behavior of $\mathbf{r}''(t)$ did for a gas. We study the solid by constructing a new kind of diagram which we call an excitation diagram. This new diagram will also prove useful in a gas, giving insight on the conditions for Ramsey fringes.

E. Excitation diagrams

The phase arising from Rule 3 can simply be added up, but it is sometimes useful to display it graphically. If we plot $\Phi_p^{\Omega}(t)$, for a single value of Ω_p, as a function of t we obtain "excitation diagrams" in the same way that "recoil diagrams" were obtained plotting $\mathbf{r}''(t)$ vs t. An excitation diagram looks just like a recoil diagram but has a different meaning. Thus the slope of each line is determined by Ω_{jp} instead of by $(\hbar/m)\mathbf{K}_{jp}$. For the two-pulse photon echo, cf. Fig. 3, the recoil and excitation diagrams are identical, for the Ramsey-fringe configurations of Figs. 4 and 7 they are not.

Excitation diagrams play the same role in solid echoes that the recoil diagrams play in gas echoes. The solid differs from the gas in two ways. First, in a solid the atoms do not move and the photon momentum is absorbed by the crystal lattice or atomic neighborhood. Second, in a solid there is a distribution in the Ω_p's that gives rise to inhomogeneous broadening. Because the atoms do not move, the recoil diagram (drawn as though the atoms were free) need not close in a solid (i.e., trajectories need not cross) in order for coherences to appear. But the excitation diagram must close in order that the phase difference $\Phi_p^{\Omega}-\Phi_{p'}^{\Omega}$ be the same for all atoms despite inhomogeneous broadening. For coherences in a gas the recoil diagram must close but the excitation diagram need not, cf. Figs. 4 and 7.

The distinction between the two diagrams becomes unnecessary for a two-level system exposed entirely to copropagating light pulses. Then Ω_{jp} is a linear function of $\mathbf{K}_{jp}$; the two cannot be varied independently. Hence if one diagram is required to close, the other also closes anyhow. In fact, in a conventional gas echo, one could regard the recoil diagram as an excitation diagram by thinking of the atoms as having sharp momenta and interpreting the Doppler effect as an inhomogeneous broadening; thus one writes $e^{i\mathbf{K}\cdot\mathbf{r}}$ as $e^{i\mathbf{K}\cdot\mathbf{v}t}$ and incorporates $\hbar\mathbf{K}\cdot\mathbf{v}$ into Ω. When any of the pulses, however, are counterpropagating, the recoil and excitation diagrams become distinct, and the behavior of a solid differs from that of a gas.

There is an additional use for the excitation diagram in studying the cumulative effect of the term $\omega_j t_j$ in Rule 2. Ramsey fringes are normally obtained in a two-level system with resonant frequency $\bar{\omega}$ by adding a variable (but j-independent) increment $\delta\omega$ to all the ω_j. The effect of this is to change $\Phi_p^{\omega}=\sum_j \Phi_{jp}^{\omega}$ (see Rule 2 or 2') by

$$\delta\Phi_p^{\omega} = -\delta\omega\sum_j \eta_{jp}t_j\ ,$$

where $\eta_{jp}=0$ or ±1 according to the cases enumerated in Rule 2 or 2'. But a study of these cases shows that η_{jp} is related to whether energy is absorbed, emitted, or neither at the jth pulse: specifically,

$$\Omega_{jp}-\Omega_{j-1p} = \bar{\omega}\eta_{jp}\ . \tag{2.14}$$

Therefore we can write

$$\frac{\delta\Phi_p^{\omega}}{\delta\omega} = -\frac{1}{\bar{\omega}}\sum_{j=1}^{n} t_j(\Omega_{jp}-\Omega_{j-1p})\ . \tag{2.15}$$

The Ramsey fringes arise from a modulation factor $e^{i(\Phi_p^{\varphi}-\Phi_{p'}^{\varphi})}$, depending through (2.15) on $\delta\omega$. (See the discussion of Rule 2.) On the other hand, the closure of the excitation diagram would mean that

$$0=\Phi_p^{\Omega}-\Phi_{p'}^{\Omega} = -\int_0^t(\Omega_p-\Omega_{p'})dt' = -\sum_{j=0}^{n}(\Omega_{jp}-\Omega_{jp'})(t_{j+1}-t_j)\ , \tag{2.16}$$

where $t_0=0$ and $t_{n+1}=t$. A Ramsey-fringe experiment normally involves a measurement of population at time t so that to have interference we must have $\Omega_{np}=\Omega_{np'}$ and $\Omega_{0p}=\Omega_{0p'}$. Therefore we may drop the terms in t_0 and t_{n+1}, obtaining

$$\Phi_p^{\Omega}-\Phi_{p'}^{\Omega}=\sum_{j=1}^{n} t_j[(\Omega_{jp}-\Omega_{jp'})-(\Omega_{j-1p}-\Omega_{j-1p'})]$$
$$=\sum_{j=1}^{n} t_j(\bar{\omega}\eta_{jp}-\bar{\omega}\eta_{jp'})$$
$$=-\bar{\omega}\left[\frac{\delta\Phi_p^{\omega}}{\delta\bar{\omega}}-\frac{\delta\Phi_{p'}^{\omega}}{\delta\bar{\omega}}\right], \quad (2.17)$$

which shows that there are no Ramsey fringes of the standard kind (right-hand side equals zero) if the excitation diagram closes (left-hand side equals zero).

It follows that the excitation diagram provides a negative criterion for the appearance of Ramsey fringes in a gas or atomic beam. Provided there is a signal, due to a crossing of trajectories in the recoil diagram, fringes will be obtained if and only if the corresponding lines do *not* cross in the excitation diagram.

This gives an easy way to see why long-term ($\tau \geq T_2^*$) Ramsey fringes are not normally obtainable from a solid. To rephase the inhomogeneous spectrum, the excitation diagram must close, and then there are no fringes. (But one might get fringes by using two lasers tuned to the same resonance and detuning only one of them.)

F. Application of rules: photon echo

Before closing this section we show how the rules apply to a standard experiment, the photon echo, Fig. 3, produced by two traveling-wave pulses in a gas. To make the application interesting, we suppose that the wave vectors of the two pulses, $\mathbf{k}_1$ and $\mathbf{k}_2$, are slightly angled from one another. We assume there is no external force

Denoting the paths p_1 and p_2 as in Fig. 3, we have for the first path Rule 1,

$$B_{1p_1}=\cos\frac{\theta_1}{2}, \quad B_{2p_1}=i\sin\frac{\theta_2}{2},$$

Rule 2,

$$\Phi_{1p_1}^{\varphi}=0, \quad \Phi_{2p_1}^{\varphi}=\mathbf{k}_2\cdot\mathbf{r}-\omega_2 t_2-\varphi_2,$$

Rule 3,

$$\Phi_{1p_1}^{\epsilon}=-(\Omega_{gr}+0)(t_2-t_1),$$
$$\Phi_{2p_1}^{\epsilon}=-\left[\Omega_{ex}+\frac{\hbar}{2m}\mathbf{k}_2^2\right](t-t_2),$$

and Rule 4,

$$\Phi_{p_1}^{\iota}=0,$$

and for the second path, Rule 1,

$$B_{1p_2}=i\sin\frac{\theta_1}{2}, \quad B_{2p_2}=i\sin\frac{\theta_2}{2},$$

Rule 2,

$$\Phi_{1p_2}^{\varphi}=\mathbf{k}_1\cdot\mathbf{r}-\omega_1 t_1-\varphi_1,$$
$$\Phi_{2p_2}^{\varphi}=-(\mathbf{k}_2\cdot\mathbf{r}-\omega_2 t_2-\varphi_2),$$

Rule 3,

$$\Phi_{1p_2}^{\epsilon}=-\left[\Omega_{ex}+\frac{\hbar}{2m}\mathbf{k}_1^2\right](t_2-t_1),$$
$$\Phi_{2p_2}^{\epsilon}=-\left[\Omega_{gr}+\frac{\hbar}{2m}(\mathbf{k}_1-\mathbf{k}_2)^2\right](t-t_2),$$

and Rule 4,

$$\Phi_{p_2}^{\iota}=0.$$

Thus Rule 5,

$$u_1u_2^*=\frac{i}{4}\sin\theta_1(1-\cos\theta_2)$$
$$\times e^{2i(\mathbf{k}_2\cdot\mathbf{r}-\omega_2 t_2-\varphi_2)-i(\mathbf{k}_1\cdot\mathbf{r}-\omega_1 t_1-\varphi_1)}$$
$$\times e^{-i(\Omega_{ex}-\Omega_{gr})(t-2t_2+t_1)}$$
$$\times e^{+i(\hbar/2m)[\mathbf{k}_1^2(t-t_1)-2\mathbf{k}_1\cdot\mathbf{k}_2(t-t_2)]}.$$

If we assume that $|\mathbf{k}_1|=|\mathbf{k}_2|=\omega/c=k$, where $\omega_1=\omega_2=\omega$ and

$$\Omega_{ex}-\Omega_{gr}=\omega-\frac{\hbar}{2m}k^2,$$

then

$$u_1u_2^*=\frac{i}{4}\sin\theta_1(1-\cos\theta_2)e^{i(2\mathbf{k}_2-\mathbf{k}_1)\cdot\mathbf{r}}e^{-i(2\varphi_2-\varphi_1)}$$
$$\times e^{-i\omega t}e^{i(\hbar/m)k^2(1-\cos\chi)(t-t_2)},$$

where χ is the angle between $\mathbf{k}_1$ and $\mathbf{k}_2$.

To apply Rule 6, we calculate the recoil displacements

$$\mathbf{r}_1''=0+\frac{\hbar}{m}\mathbf{k}_2(t-t_2),$$
$$\mathbf{r}_2''=\frac{\hbar}{m}\mathbf{k}_1(t_2-t_1)+\frac{\hbar}{m}(\mathbf{k}_1-\mathbf{k}_2)(t-t_2),$$

and obtain

$$\Delta\mathbf{r}''=\mathbf{r}_1-\mathbf{r}_2=2\frac{\hbar}{m}(\mathbf{k}_2-\mathbf{k}_1)(t_2-t_1)$$
$$+\frac{\hbar}{m}(2\mathbf{k}_2-\mathbf{k}_1)(t-2t_2+t_1).$$

If χ is small then $\mathbf{k}_2-\mathbf{k}_1$ is almost perpendicular to $2\mathbf{k}_2-\mathbf{k}_1$, and we have Rule 6,

$$f_{p_1p_2}\cong e^{-4(k_BT/2m)(\mathbf{k}_2-\mathbf{k}_1)^2(t_2-t_1)^2}$$
$$\times e^{-(k_BT/2m)(2\mathbf{k}_2-\mathbf{k}_1)^2(t-2t_2+t_1)^2}$$
$$\cong e^{-4\chi^2(k_BT/2m)k^2(t_2-t_1)^2}$$
$$\times e^{-(k_BT/2m)k^2(t-2t_2+t_1)^2}.$$

The first factor represents the failure of the diagram to close exactly at the echo time $t=2t_2-t_1$, because of the angle between the two pulses. Thus the two trajectories miss each other slightly in 3-space. The second factor gives the ordinary T_2^* suppression of the echo before and

after the echo time.

In $u_1 u_2^*$ we see the usual factor $\sin\theta_1(1-\cos\theta_2)$ relating the amplitude of the echo to the pulse areas. The factor

$$e^{-i\omega t} e^{i(\hbar/m)k^2(1-\cos\chi)(t-t_2)}$$

tells us that the echo emission will have frequency $\omega^\bullet=\omega-(\hbar/m)k^2(1-\cos\chi)$. The factor $e^{i(2\mathbf{k}_2-\mathbf{k}_1)\cdot\mathbf{r}}$ tells us that the echo will be directed along $2\mathbf{k}_2-\mathbf{k}_1$, but since the frequency requires that $|\mathbf{k}|=\omega^\bullet/c\cong k$, there is a slight mismatch in $\langle\langle \mathbf{P}e^{-i\mathbf{k}\cdot\mathbf{r}}\rangle\rangle$:

$$2\mathbf{k}_2-k_1-k=k(\sqrt{5-4\cos\chi}-1)$$

$$\cong 2(1-\cos\chi)\mathbf{k} .$$

This will suppress the echo if the sample length exceeds $\approx 1/k\chi^2$. [We have neglected $(\omega^\bullet-\omega)/c$ which is smaller by $\hbar k/mc$.]

The reader accustomed to conventional calculations, based for example on the density matrix, will recognize all the factors above. We are not presenting a rival theory, only a way of connecting conventional calculations to a pictorial model.

III. THEORY

A. Gas of a single atom

The theoretical development we present immediately below is for a gas of many atoms. We do this for convenience only. If one uses homodyne detection in measuring radiated signals or if one detects atomic populations the results obtained below will hold for repeated experiments performed on a gas of a single atom, cf. Appendix A.

B. Atomic beams

Although our analysis will refer to a gas, the results hold as well for an atomic beam, as will be discussed in Appendix B.

C. Gas of many atoms

Our aim is to derive the "Feynman rules" given in Sec. II D and to justify the "substitute wave packet" derived in (2.3). We begin by considering an ensemble of atoms in a gaseous state with a wave function

$$\psi(\mathbf{r}_1,\ldots\mathbf{r}_N,t)=\prod_s \Psi_s(\mathbf{r}_s,t) , \tag{3.1}$$

where s runs over the N individual atoms.

We remind the reader that our sample is assumed to be optically thin and therefore every atom can be assumed to be affected by the same classically described, suitably retarded pulse, *independently of how the other atoms have reacted.* The pulses therefore introduce no correlations between atoms and the gas remains in a product state throughout the experiment [17].

For each atom we decompose the wave function according to

$$\Psi_s(\mathbf{r},t)=\sum_p \psi_{snp}(\mathbf{r},t)|np\rangle_s , \tag{3.2}$$

where n is the number of optical pulses that have been applied up to the time t, and p labels the path leading to that state. It follows that

$$\Psi_s^\dagger(\mathbf{r},t)=\sum_p \psi_{snp}^*(\mathbf{r},t)_s\langle np| . \tag{3.3}$$

The notion of path is as follows. Each time an optical pulse is applied an optical transition may be induced and the wave function may begin to evolve for the new internal state as well as for the old one from which it came. After a series of pulses the wave function is expressed as a linear combination of internal kets with r-dependent coefficients. We follow them all keeping track of internal history. Thus there may be more than one value of p for any value of n. The energy of the np state is given by $\hbar\Omega_{np}$. In Fig. 8 we present a possible labeling scheme. (This scheme is not used consistently throughout the paper.)

1. *Evolution of a wave packet*

Our plan is to introduce external forces and fields but we wish to start with the free-particle case and introduce these complications later. We therefore start out with the atoms in the ground state and express the external wave function of the sth atom as a wave packet

$$\psi_s(\mathbf{r},t)=\int d^3\mathbf{q}\, A_s(\mathbf{q}) \times e^{i[\mathbf{q}\cdot(\mathbf{r}-\mathbf{R}_s)-\Omega_0 t-(\hbar/2m)\mathbf{q}^2 t]} , \tag{3.4}$$

where $\mathbf{q}$ is a dummy momentum variable and $\mathbf{R}_s$ is the initial position of the center of mass of the wave packet. The probability distribution of momentum states from which the wave packet is constructed is given by $|A_s(\mathbf{q})|^2$.

To facilitate expressing the wave function after multipulse excitation we rewrite (3.4) as

$$\psi_{s0p}(r,t)=\int d^3\mathbf{q}\, A_s(\mathbf{q}) e^{i\mathbf{q}\cdot(\mathbf{r}-\mathbf{R}_s)} \tilde{B}_{0p}(\mathbf{r},\mathbf{q},t) , \tag{3.5}$$

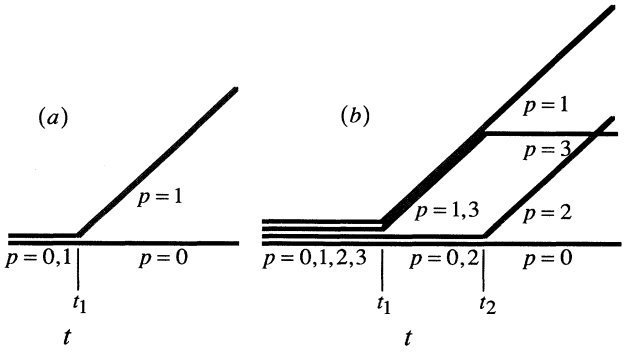

FIG. 8. Label scheme. We assign an index p to each path which leads to a distinct wave function $\psi_p(t)$. Each laser pulse has the potential for generating additional wave packets.

where

$$\tilde{B}_{0p}(\mathbf{r},\mathbf{q},t)=e^{-i[\Omega_{0p}+(\hbar/2m)\mathbf{q}^2]t} . \tag{3.6}$$

We have included the superfluous argument $\mathbf{r}$ for consistency: see (3.8).

Effect of single-pulse excitation. The application of a resonant optical pulse with wave vector $\mathbf{k}_1$ leads to, cf. Appendix C,

$$\psi_{s1p}(\mathbf{r},t)=\int d^3\mathbf{q}\, A_s(\mathbf{q})e^{i\mathbf{q}\cdot(\mathbf{r}-\mathbf{R}_s)} \times\tilde{B}_{1p}(\mathbf{r},\mathbf{q},t)\tilde{B}_{0p}(\mathbf{r},\mathbf{q},t_1) , \tag{3.7}$$

where

$$\tilde{B}_{1p}(\mathbf{r},\mathbf{q},t)=B_{1p}e^{+i(\tilde{k}_{1p}\cdot\mathbf{r}-\tilde{\omega}_{1p}t_1-\tilde{\varphi}_{1p})} \times e^{-i(\Omega_{1p}+(\hbar/2m)(\mathbf{q}+\tilde{\mathbf{k}}_{1p})^2](t-t_1)} . \tag{3.8}$$

In the most usual case (see Rule 1 and Appendix C)

$$B_{jp}=1 \text{ or } \cos\frac{\theta_j}{2} \text{ or } i\sin\frac{\theta_j}{2} , \tag{3.9}$$

where θ_j is the area [2] of the optical pulse. Equation (3.9) depends on whether (1) the pulse does not connect with the energy level; (2) the pulse connects and leaves the atomic state unchanged; (3) the pulse connects and changes the atomic state. For completeness we set $B_{0p}=1$.

We have also used

$$\begin{aligned}\tilde{\omega}_{jp}&=0 \text{ or } +\omega_j \text{ or } -\omega_j,\\ \tilde{\mathbf{k}}_{jp}&=0 \text{ or } +\mathbf{k}_j \text{ or } -\mathbf{k}_j ,\\ \tilde{\phi}_{jp}&=0 \text{ or } +\phi_j \text{ or } -\phi_j ,\end{aligned} \tag{3.10}$$

where $\omega_j=k_jc$ is the frequency of the jth pulse and the pulse phase is $\mathbf{k}_j\cdot\mathbf{r}-\omega_jt_j-\phi_j$. Equation (3.10) depends on whether (1) the pulse applied does not change the atomic state; (2) the pulse changes the atomic state because of absorption; (3) the pulse changes the atomic state because of stimulated emission. Note that this is *not* the same classification of outcomes that determines (3.9).

Multipulse development. Following a series of n optical excitation pulses the general wave-function component becomes

$$\psi_{snp}(\mathbf{r},t)=\int d^3\mathbf{q}\, A_s(\mathbf{q})e^{-i\mathbf{q}\cdot(\mathbf{r}-\mathbf{R}_s)}\tilde{B}_{np}(\mathbf{r},\mathbf{q},t) \times\tilde{B}_{n-1p}(\mathbf{r},\mathbf{q},t_n)\cdots\tilde{B}_{0p}(\mathbf{r},\mathbf{q},t_1) , \tag{3.11}$$

where

$$\tilde{B}_{jp}(\mathbf{r},\mathbf{q},t)=B_{jp}e^{+i(\tilde{\mathbf{k}}_{jp}\cdot\mathbf{r}-\tilde{\omega}_{jp}t_j-\tilde{\varphi}_{jp})}\exp\left\{-\left[\Omega_{jp}+\frac{\hbar}{2m}\left[q+\sum_{j'=1}^{j}\tilde{\mathbf{k}}_{j'p}\right]^2\right](t-t_j)\right\} . \tag{3.12}$$

If we introduce the definitions

$$\mathbf{K}_p(t)\equiv\sum_{j=1}^{t_j<t}\tilde{\mathbf{k}}_{jp} \tag{3.13}$$

and

$$\Omega_p=\Omega_p(t)\equiv\Omega_{jp} , \tag{3.14a}$$

where j is chosen so that

$$t_j<t<t_{j+1} , \tag{3.14b}$$

the wave packet can be rewritten as

$$\Psi_{snp}(\mathbf{r},t)=B_p\int d^3\mathbf{q}\, A_s(\mathbf{q})e^{i[\mathbf{q}\cdot(\mathbf{r}-\mathbf{R}_s)+\mathbf{K}_p\cdot\mathbf{r}-\Phi_p^{\omega}]}\exp\left[-i\int_0^t\left[\Omega_p(t')+\frac{\hbar}{2m}[\mathbf{q}+\mathbf{K}_p(t')]^2\right]dt'\right] , \tag{3.15}$$

where

$$B_p=B_p(t)\equiv\prod_{j}^{t_j(<t)}B_{jp} \tag{3.16}$$

and

$$\Phi_p^{\omega}=\sum_{j'=1}^{j}(\tilde{\omega}_{j'p}t_{j'}+\tilde{\varphi}_{j'p}) . \tag{3.17}$$

The combination $\mathbf{K}_p\cdot\mathbf{r}-\Phi_p^{\omega}$ is just the cumulative sum of the phases Φ_p^{φ} defined in Sec. II D, Rule 2.

Introduction of generalized forces and fields. We allow for the presence of generalized forces and fields by introducing the variable

$$\mathbf{Q}=\mathbf{Q}(t)=\mathbf{q}+\mathbf{q}'(t) , \tag{3.18}$$

where $\mathbf{q}'(t)$ represents the classical motion induced by such forces [that is, $\mathbf{q}'(0)=0$ and $\hbar\dot{\mathbf{q}}'=\mathbf{F}_{\text{external}}$]. We will consider two distinct cases later. It is easily seen that the effect of $\mathbf{F}_{\text{external}}$ on (3.15) is, first, to replace $\mathbf{q}\cdot(\mathbf{r}-\mathbf{R}_s)$ by $\mathbf{Q}\cdot(\mathbf{r}-\mathbf{R}_s)$, and second, to replace $\mathbf{q}+\mathbf{K}_p(t')$ by $\mathbf{Q}(t')+\mathbf{K}_p(t')$. With these substitutions the generalized wave-function component is simply expressed as

$$\Psi_p(\mathbf{r},t)=B_p\int d^3\mathbf{q}\, A_s(\mathbf{q})e^{i[\mathbf{Q}\cdot(\mathbf{r}-\mathbf{R}_s)+\mathbf{K}_p\cdot\mathbf{r}-\Phi_p^{\omega}]} \times\exp\left[-i\int_0^t\left[\Omega_p+\frac{\hbar}{2m}(\mathbf{Q}+\mathbf{K}_p)^2\right]\right]dt' . \tag{3.19}$$

The subscript n has also been suppressed since it is to be understood that all excitation pulses applied up to the time t have been included.

The discussion up to now has assumed only traveling-wave pulses, but it is evident from the last part of Appendix C that (3.19) with (3.16) and (3.17) holds if for each standing-wave pulse we set

$$\tilde{\omega}_{jp}=\eta\omega_{jp} , \tag{3.20}$$

$$\tilde{\varphi}_{jp}=m\frac{\varphi_j^+-\varphi_j^-}{2}+\eta\frac{\varphi_j^++\varphi_j^-}{2} \tag{3.21}$$

in accordance with Rule (2′) in Sec. II F and define B_{jp} in accordance with Rule (1′).

2. *Expectation values and two-path coherence*

The effect and object of applying a series of resonant optical pulses on a gaseous ensemble of atoms is (1) to produce a radiated signal

$$\mathbf{E}(\mathbf{k})=k^2\frac{e^{ik\cdot R}}{R}\int d^3\mathbf{r}\langle \mathbf{P}e^{-i\mathbf{k}\cdot\mathbf{r}}\rangle$$
$$=k^2\frac{e^{ik\cdot R}}{R}\langle\langle \mathbf{P}e^{-i\mathbf{k}\cdot\mathbf{r}}\rangle\rangle , \tag{3.22}$$

where $\mathbf{R}$ is the distance between the detector and the sample $\mathbf{k}\|\mathbf{R}$ is the wave vector of the radiation signal, and $\mathbf{P}=\mathbf{P}(\mathbf{r})$ is the dipole moment operator

$$\mathbf{P}(\mathbf{r})=\mathbf{p}\sum_s |\mathrm{gr}\rangle_s\delta(\mathbf{r}_s-\mathbf{r})_s\langle \mathrm{ex}|\prod_{s'(\neq s)}\mathbb{1}_{s'} \tag{3.23}$$

(here $\mathbf{p}\perp\mathbf{k}$ is the appropriate dipole moment matrix element of a single atom, and $\mathbf{r}_s$ is the position operator of the s atom). (We shall henceforth omit the factor $\prod_{s'(\neq s)}\mathbb{1}_{s'}$.) Then

$$\langle\langle \mathbf{P}e^{-i\mathbf{k}\cdot\mathbf{r}}\rangle\rangle=\mathrm{Tr}(\mathbf{P}_{\mathbf{k}}\rho) , \tag{3.24}$$

where ρ is the density matrix and

$$\mathbf{P}_{\mathbf{k}}\equiv\sum_s |\mathrm{gr}\rangle_s\mathbf{p}e^{-i\mathbf{k}\cdot\mathbf{r}_s}{}_s\langle \mathrm{ex}| ; \tag{3.25}$$

or (2) to develop an excited-state population

$$\langle\langle N_{\mathrm{ex}}\rangle\rangle=\mathrm{Tr}(N_{\mathrm{ex}}\rho) , \tag{3.26}$$

where

$$N_{\mathrm{ex}}=\sum_s |\mathrm{ex}\rangle_s{}_s\langle \mathrm{ex}| . \tag{3.27}$$

In the former case we write $\mathrm{Tr}_{(s)}$ for the trace over the states of atom s and obtain

$$\langle\langle \mathbf{P}e^{-i\mathbf{k}\cdot\mathbf{r}}\rangle\rangle=\sum_s \mathrm{Tr}_{(s)}(|\mathrm{gr}\rangle_s\mathbf{p}e^{-i\mathbf{k}\cdot\mathbf{r}_s}{}_s\langle \mathrm{ex}|\Psi_s\Psi_s^\dagger)$$
$$=\mathbf{p}\sum_s\int d^3\mathbf{r}\,e^{-i\mathbf{k}\cdot\mathbf{r}}{}_s\langle \mathrm{ex}|\Psi_s(\mathbf{r},t)\Psi_s^\dagger(\mathbf{r},t)|\mathrm{gr}\rangle_s$$
$$=p\sum_s\int d^3\mathbf{r}\,e^{-i\mathbf{k}\cdot\mathbf{r}}\sum_{p_1,p_2}{}_s\langle \mathrm{ex}|np_1\rangle_s{}_s\langle np_2|\mathrm{gr}\rangle_s\psi_{snp_1}(\mathbf{r},t)\psi^*_{snp_2}(\mathbf{r},t)$$
$$=p\sum_s\int d^3\mathbf{r}\,e^{-i\mathbf{k}\cdot\mathbf{r}}\sum_{p_1}^{\mathrm{ex}}\sum_{p_2}^{\mathrm{gr}}\psi_{snp_1}(\mathbf{r},t)\psi^*_{snp_2}(\mathbf{r},t) , \tag{3.28}$$

where $\sum_p^{\mathrm{ex}}$ denotes the sum over paths p that terminate in the excited state, and likewise $\sum_p^{\mathrm{gr}}$. Our derivation of (3.28) is simplified by using short-hand notation [19].

In a similar manner we find

$$\langle\langle N_{\mathrm{ex}}\rangle\rangle=\sum_s\int d^3\mathbf{r}\sum_{p_1}^{\mathrm{ex}}\sum_{p_2}^{\mathrm{ex}}\psi_{snp_1}(\mathbf{r})\psi^*_{snp_2}(\mathbf{r}) . \tag{3.29}$$

Matrix element evaluation. To evaluate either (3.28) or (3.29) we write

$$\langle\langle \mathbf{P}e^{-i\mathbf{k}\cdot\mathbf{r}}\rangle\rangle=\mathbf{p}\sum_{p_1}^{\mathrm{ex}}\sum_{p_2}^{\mathrm{gr}}M_{p_1p_2}(\mathbf{k}) , \tag{3.30}$$

$$\langle\langle N_{\mathrm{ex}}\rangle\rangle=\sum_{p_1}^{\mathrm{ex}}\sum_{p_2}^{\mathrm{ex}}M_{p_1p_2}(0) , \tag{3.31}$$

where

$$M_{p_1p_2}(\mathbf{k})=\sum_s\int d^3\mathbf{r}\,e^{-i\mathbf{k}\cdot\mathbf{r}}\psi_{snp_1}(\mathbf{r},t)\psi^*_{snp_2}(\mathbf{r},t)$$
$$=B_{p_1}B^*_{p_2}\sum_s\int d^3\mathbf{r}\,e^{i(\mathbf{K}_{p_1}-\mathbf{K}_{p_2}-k)\cdot r}e^{-i(\Phi^\omega_{p_1}-\Phi^\omega_{p_2})}$$
$$\times\int d^3\mathbf{q}_1d^3\mathbf{q}_2A_s(\mathbf{q}_1)A_s^*(\mathbf{q}_2)e^{i(\mathbf{Q}_1-\mathbf{Q}_2)\cdot(\mathbf{r}-\mathbf{R}_s)}$$
$$\times\exp\left[-i\int_0^t\left[\Omega_{p_1}+\frac{\hbar}{2m}(\mathbf{Q}_1+\mathbf{K}_{p_1})^2-\Omega_{p_2}-\frac{\hbar}{2m}(\mathbf{Q}_2+\mathbf{K}_{p_2})^2\right]dt'\right] . \tag{3.32}$$

We now assume that there is no correlation, in the ensemble of atoms, between the position $\mathbf{R}_s$ and the momentum amplitude $A_s(\mathbf{q})$. (We shall refer to this as the homogeneity assumption.) Thus the sum

$$\sum_s A_s(\mathbf{q}_1)A_s^*(\mathbf{q}_2)e^{i(\mathbf{Q}_1-\mathbf{Q}_2)\cdot(\mathbf{r}-\mathbf{R}_s)}$$

can be replaced by

$$(1/N)\sum_{s,s'} A_s(\mathbf{q}_1)A_s^*(\mathbf{q}_2)e^{i(\mathbf{Q}_1-\mathbf{Q}_2)\cdot(\mathbf{r}-\mathbf{R}_{s'})} .$$

The summation over $\mathbf{R}_{s'}$, for N atoms distributed quasiuniformly in a volume V, yields a δ function

$$\sum_{s'} e^{i(\mathbf{Q}_1-\mathbf{Q}_2)\cdot\mathbf{R}_{s'}}=(2\pi)^3\frac{N}{V}\delta(\mathbf{Q}_1-\mathbf{Q}_2) \tag{3.33}$$

which can be reexpressed as

$$\sum_{s'} e^{i(\mathbf{Q}_1-\mathbf{Q}_2)\cdot\mathbf{R}_{s'}}=(2\pi)^3\frac{N}{V}\delta(\mathbf{q}_1-\mathbf{q}_2) \tag{3.34}$$

since $\mathbf{q}'$ is independent of path. It follows that the only dependence on $\mathbf{r}$ is in the factor $e^{i(\mathbf{K}_{p_1}-\mathbf{K}_{p_2}-\mathbf{k})\cdot\mathbf{r}}$ and the integration over $\mathbf{r}$ yields

$$\int d^3\mathbf{r}\, e^{i(\mathbf{K}_{p_1}-\mathbf{K}_{p_2}-\mathbf{k})\cdot\mathbf{r}}=V\delta_{\mathbf{K}_{p_1}-\mathbf{K}_{p_2}-\mathbf{k}} . \tag{3.35}$$

We write therefore

$$\begin{aligned}M_{p_1p_2}(\mathbf{k})=&(2\pi)^3\delta_{\mathbf{K}_{p_1}-\mathbf{K}_{p_2}-\mathbf{k}}B_{p_1}B_{p_2}^*e^{-i(\Phi^\omega_{p_1}-\Phi^\omega_{p_2})}\\&\times\sum_s\int d^3\mathbf{q}_1 d^3\mathbf{q}_2\, A_s(\mathbf{q}_1)A_s^*(\mathbf{q}_2)\delta(\mathbf{q}_1-\mathbf{q}_2)\\&\times\exp\left[-i\int_0^t\left[\Omega_{p_1}+\frac{\hbar}{2m}(\mathbf{Q}_1+\mathbf{K}_{p_1})^2-\Omega_{p_2}-\frac{\hbar}{2m}(\mathbf{Q}_2+\mathbf{K}_{p_2})^2\right]dt'\right] ,\end{aligned} \tag{3.36}$$

which on using

$$\begin{aligned}(\mathbf{Q}+\mathbf{K}_{p_1})^2-(\mathbf{Q}+\mathbf{K}_{p_2})^2&=2\mathbf{Q}\cdot(\mathbf{K}_{p_1}-\mathbf{K}_{p_2})+(\mathbf{K}_{p_1}^2-\mathbf{K}_{p_2}^2)\\&=2(\mathbf{q}+\mathbf{q}')\cdot(\mathbf{K}_{p_1}-\mathbf{K}_{p_2})+(\mathbf{K}_{p_1}^2-\mathbf{K}_{p_2}^2)\end{aligned} \tag{3.37}$$

can be rewritten as

$$\begin{aligned}M_{p_1p_2}(\mathbf{k})=&(2\pi)^3N\delta_{\mathbf{K}_{p_1}-\mathbf{K}_{p_2}-\mathbf{k}}B_{p_1}B_{p_2}^*e^{-i(\Phi^\omega_{p_1}-\Phi^\omega_{p_2})}\\&\times\exp\left[-i\int_0^t\left[\Omega_{p_1}+\frac{\hbar}{2m}\mathbf{K}_{p_1}^2-\Omega_{p_2}-\frac{\hbar}{2m}\mathbf{K}_{p_2}^2\right]dt'\right]\exp\left[-i\frac{\hbar}{m}\int_0^t\mathbf{q}'\cdot(\mathbf{K}_{p_1}-\mathbf{K}_{p_2})dt'\right]\\&\times\int d^3\mathbf{q}\, A^*(\mathbf{q})A(\mathbf{q})\exp\left[-i\frac{\hbar}{m}\mathbf{q}\cdot\int_0^t(\mathbf{K}_{p_1}-\mathbf{K}_{p_2})dt'\right] ,\end{aligned} \tag{3.38}$$

where we have defined $A(\mathbf{q})$ by

$$|A(\mathbf{q})|^2=\frac{1}{N}\sum_s|A_s(\mathbf{q})|^2,\quad A(\mathbf{q})\text{real}>0 . \tag{3.39}$$

This calculation has shown that the consequence of the homogeneity assumption made after (3.32) is the same as if we had replaced each $A_s(\mathbf{q})$ in the first place by the s-independent function $A(\mathbf{q})$. It is clear from (3.39) that $|A(\mathbf{q})|^2$ is the actual distribution function of the atoms in momentum space. For a gas in thermal equilibrium we may take this to be the Maxwell-Boltzmann distribution.

3. *Justification of billiard model*

The exponential in $\mathbf{q}$ [last factor in (3.38)] involves only the recoil displacement

$$\mathbf{r}_p''\equiv\frac{\hbar}{m}\int_0^t\mathbf{K}_p dt' . \tag{3.40}$$

The preceding two exponential factors may be treated concisely by defining

$$\Phi_p^\iota \equiv -\frac{\hbar}{m}\int_0^t \mathbf{q}'\cdot\mathbf{K}_p dt' = -\int_0^t \mathbf{q}'\cdot d\mathbf{r}_p'' \tag{3.41}$$

and

$$\Phi_p^\epsilon \equiv -\int_0^t \left[\Omega_p + \frac{\hbar}{2m}\mathbf{K}_p^2\right] dt' \ . \tag{3.42}$$

This latter term, dominated by Ω_p, we call the excitation phase. With these definitions our result is more concisely expressed as

$$M_{p_1p_2}(\mathbf{k}) = (2\pi)^3 N \delta_{\mathbf{K}_{p_1}-\mathbf{K}_{p_2}-\mathbf{k}} B_{p_1} B_{p_2}^* \times e^{i(-\Delta\Phi^\omega_{p_1p_2}+\Delta\Phi^\epsilon_{p_1p_2}+\Delta\Phi^\iota_{p_1p_2})} \times \int d^3\mathbf{q}\, A^*(\mathbf{q}) A(\mathbf{q}) e^{-i\mathbf{q}\cdot(\mathbf{r}''_{p_1}-\mathbf{r}''_{p_2})} , \tag{3.43}$$

where we have used

$$\Delta\Phi_{p_1p_2} \equiv \Phi_{p_1} - \Phi_{p_2} \ . \tag{3.44}$$

A glance at (3.43) shows that if $|A_s(\mathbf{q})|^2$ is spread over a wide range $\Delta\mathbf{q}$, the integral over $\mathbf{q}$ will be small unless $|\mathbf{r}''_{p_1}-\mathbf{r}''_{p_2}| \le |\Delta\mathbf{q}|^{-1}$, which is what we call the "size" of the billiard ball. This is equivalent to saying that the recoil diagram must close. Note that $\mathbf{r}_p''$ is due only to photon recoil; that is why the recoil diagrams are drawn with straight lines even if an external force is present.

Substitute wave function. Another way of understanding the simplification that results from comparing two paths is to repeat the procedure of (3.36)–(3.43) for the wave function itself. Starting with (3.19) but making the replacement $A_s(\mathbf{q}) \to A(\mathbf{q})$ in accordance with the homogeneity assumption [see (3.39)] and then expanding

$$(\mathbf{Q}+\mathbf{K}_p)^2 = (\mathbf{q}+\mathbf{q}'+\mathbf{K}_p)^2 = q^2+2\mathbf{q}\cdot\mathbf{q}'+q'^2+2\mathbf{q}\cdot\mathbf{K}_p+2\mathbf{q}'\cdot\mathbf{K}_p+K_p^2 \ , \tag{3.45}$$

one obtains

$$\psi_{sp}(\mathbf{r},t) = B_p \int d^3\mathbf{q}\, A(\mathbf{q}) e^{i[\mathbf{q}+\mathbf{q}'(t)]\cdot(\mathbf{r}-\mathbf{R}_s)} e^{i(\mathbf{K}_p\cdot\mathbf{r}-\Phi_p^\omega+\Phi_p^\epsilon+\Phi_p^\iota)} \exp\left[-i\frac{\hbar}{2m}\int_0^t dt'(q^2+2\mathbf{q}\cdot\mathbf{q}'+q'^2+2\mathbf{q}\cdot\mathbf{K}_p)\right] , \tag{3.46}$$

where Φ_p^ω, Φ_p^ϵ, Φ_p^ι are as previously defined.

We now introduce the function of space and time

$$F(\mathbf{r}-\mathbf{R}_s,t) \equiv \int d^3\mathbf{q}\, A(\mathbf{q}) \times e^{i(\mathbf{q}\cdot(\mathbf{r}-\mathbf{R}_s)-(\hbar/2m)\mathbf{q}^2 t]} , \tag{3.47}$$

which represents a wave packet with initial momentum distribution $A(\mathbf{q})$ and center of mass $\mathbf{R}_s$ after evolution through a time t in the *absence* of any external forces or pulses.

Defining

$$\mathbf{r}'(t) = \int \frac{\hbar}{m}\mathbf{q}'dt' \ , \tag{3.48}$$

we see that (3.46) can be rewritten as

$$\psi_{sp}(\mathbf{r},t) = B_p e^{i(\mathbf{K}_p\cdot\mathbf{r}-\Phi_p^\omega+\Phi_p^\epsilon+\Phi_p^\iota+\Phi^\xi)} \times F(\mathbf{r}-\mathbf{r}'(t)-\mathbf{r}''(t)-\mathbf{R}_s,t) \ , \tag{3.49}$$

where

$$\Phi^\xi = \mathbf{q}'\cdot(\mathbf{r}-\mathbf{R}_s) - \frac{\hbar}{2m}\int_0^t q'^2 dt' \tag{3.50}$$

is an additional phase independent of p.

If we use this expression to evaluate $M_{p_1p_2}$ [first line of (3.32)] we obtain (3.43). But in doing so we observe three cancellations: the factor

$$e^{i\mathbf{q}'\cdot(\mathbf{r}-\mathbf{R}_s)} \exp\left[-\frac{\hbar}{2m}\int_0^t Q^2 dt'\right] = \exp\left[-i\frac{\hbar}{2m}q^2 t\right] e^{-i\mathbf{q}\cdot\mathbf{r}'(t)} e^{i\Phi^\xi}$$

is the same for both paths, and therefore this factor could have been dropped from ψ_{sp} *without affecting the result.* Without this factor, ψ_{sp} becomes

$$\hat{\psi}_{sp}(\mathbf{r},t) = B_p e^{i(\mathbf{K}_p\cdot\mathbf{r}-\Phi_p^\omega+\Phi_p^\epsilon+\Phi_p^\iota)} F(\mathbf{r}-\mathbf{r}''(t)-\mathbf{R}_s,0) \ . \tag{3.51}$$

We call $\hat{\psi}_{sp}$ the *substitute wave packet.* It describes recoil due *only* to photon impact, and with *no* diffractive spreading.

If we now write (3.32) in terms of $\hat{\psi}_{sp}$ we have

$$M_{p_1p_2}(\mathbf{k}) = B_{p_1}B_{p_2}^* e^{i(-\Delta\Phi^\omega_{p_1p_2}+\Delta\Phi^\epsilon_{p_1p_2}+\Delta\Phi^\iota_{p_1p_2})} \times \sum_s \int d^3\mathbf{r}\, e^{i(\mathbf{K}_{p_1}-\mathbf{K}_{p_2}-\mathbf{k})\cdot\mathbf{r}} F(\mathbf{r}-\mathbf{r}''_{p_1}-\mathbf{R}_s,0) F^*(\mathbf{r}-\mathbf{r}''_{p_2}-\mathbf{R}_s,0) \ . \tag{3.52}$$

In this form the requirement of closure of the recoil diagram ($\mathbf{r}''_{p_1}=\mathbf{r}''_{p_2}$) is exhibited as a literal overlap of the "billiard balls" defined by the extent of the function $F(\mathbf{r}-\mathbf{r}''-\mathbf{R}_s,0)$. The central point of the billiard ball, $\mathbf{R}_s+\mathbf{r}''(t)=\mathbf{R}_s+(\hbar/m)\int_0^t \mathbf{K}_p dt'$, is defined by imagining a classical atom initially at rest and subject to photon impacts

but not to external forces.

Note that the substitute wave packet $\hat{\psi}_{sp}(\mathbf{r},t)$, on which the billiard-ball model is based, differs from the true one in three respects: the compression of the wave packet due to the replacement of $A_s(\mathbf{q})$ by $A(\mathbf{q})$, the omission of diffractive spread achieved by setting $t\rightarrow 0$ in the second argument of F, and the omission of the path-independent phases Φ^{ξ} and $\mathbf{q}'\cdot\mathbf{r}'$ arising from external force. We do not necessarily assert that the substitute wave function $\hat{\Psi}_s(\mathbf{r},t)=\sum_p \hat{\psi}_{sp}(\mathbf{r},t)|np\rangle_s$ correctly describes the sth atom, only that under very general assumptions the experimental quantities $\langle\langle \mathbf{P}e^{-i\mathbf{k}\cdot\mathbf{r}}\rangle\rangle$ and $\langle\langle N_{\rm ex}\rangle\rangle$ can be calculated *as though* the atoms were all in their "substitute" states as depicted by the BBM.

For later reference we write out the substitute wave function with the last two phase terms expressed in terms of their definitions

$$\hat{\psi}_{sp}(\mathbf{r},t)=B_p\exp\left\{i\left[\mathbf{K}_p\cdot\mathbf{r}-\Phi_p^{\omega}-\int_0^t\left[\Omega_p+\frac{\hbar}{2m}\mathbf{K}_p^2\right]dt'-\int_0^t\mathbf{q}'\cdot d\mathbf{r}_p''\right]\right\}F(\mathbf{r}-\mathbf{r}_p''-\mathbf{R}_s,0)\ . \tag{3.53}$$

Rules 1–3. Equation (3.50) shows that in calculating coherence effects the diffractive spreading of the wave packets is of no consequence. It suffices to follow the unspread wave packet to discover when coherences occur. Having determined when coherences exist it then is necessary to evaluate the phase factors associated with the wave packet.

The factors B_p, $e^{i(\mathbf{K}_p\cdot\mathbf{r}-\Phi_p^{\omega})}\equiv e^{i\Phi_p^{\varphi}}$, and

$$\exp\left[-i\int_0^t\left[\Omega_p+\frac{\hbar}{2m}\mathbf{K}_p^2\right]dt'\right]\equiv e^{i\Phi_p^{\epsilon}}$$

yield Rules 1–3, respectively.

Following the wave packets means following the path $\mathbf{r}''$ defined by (3.40). A plot of $\mathbf{r}''$ as a function of t is what is meant by a recoil diagram.

Wave function in a solid. In a solid there is no recoil and the wave function is just

$$\hat{\Psi}_{sp}(\mathbf{r},t)=B_p\exp\left[i\left[\mathbf{K}_p\cdot\mathbf{R}_s-\Phi_p^{\omega}-\int_0^t\Omega_p dt'\right]\right]G(\mathbf{r}-\mathbf{R}_s)\ . \tag{3.54}$$

The atoms are localized at the lattice sites according to $G(\mathbf{r}-\mathbf{R}_s)$ and the electronic frequencies Ω_p are distributed according to the inhomogeneous spread of lattice strains at the various sites. Recoil diagrams do not apply and are replaced by excitation diagrams (Sec. II E) which plot the excitation phase $\int_0^t\Omega_p(t')dt'$ as a function of t.

Force-field phase—Rule 4. The effect of external forces or fields is to introduce a phase factor (3.41) which can be interpreted in terms of the recoil trajectories. We write this factor as

$$\begin{aligned}\Phi_p^{\iota}&=-\int_0^t\mathbf{q}'\cdot d\mathbf{r}_p''\\&=-\mathbf{q}'\cdot\mathbf{r}_p''\big|_0^t+\int_0^t\mathbf{r}_p''\cdot d\mathbf{q}'\\&=-q'(t)\cdot\mathbf{r}_p''(t)+\int_0^t\mathbf{r}_p''\cdot\dot{\mathbf{q}}'dt'\\&=-\mathbf{q}'\cdot\mathbf{r}_p''+\int_0^t\dot{\mathbf{q}}'\cdot d\,\mathbf{A}_p\ ,\end{aligned} \tag{3.55}$$

where $\mathbf{r}_p''dt\equiv d\,\mathbf{A}_p$. For constant acceleration such as produced by a constant gravitational field or constant rotary motion, the above result reduces in accordance with Rule 4 to

$$\Phi_p^{\iota}=-\mathbf{q}'\cdot\mathbf{r}_p''+\dot{\mathbf{q}}'\cdot\mathbf{A}_p\ , \tag{3.56}$$

where

$$\mathbf{A}_p=\int_0^t d\,\mathbf{A}_p=\int_0^t\mathbf{r}_p''dt'\ . \tag{3.57}$$

Thus if all the photon momenta are directed along one line (not necessarily all in the same sense) the difference $\dot{\mathbf{q}}'\cdot(\mathbf{A}_{p_1}-\mathbf{A}_{p_2})=\dot{\mathbf{q}}'\cdot\mathbf{A}_{p_1p_2}$ is just the area enclosed between paths p_1 and p_2 in the recoil diagram. (3.56) is equivalent to (2.9) since $\dot{\mathbf{q}}'=m\dot{\mathbf{v}}/\hbar$. We further note that at the trajectory crossings the term $\mathbf{q}'\cdot\mathbf{r}_p''$ drops out and we obtain

$$\Delta\Phi_{p_1p_2}^{\iota}=\dot{\mathbf{q}}'\cdot\mathbf{A}_{p_1p_2}\ . \tag{3.58}$$

Rule 5. Using the phase factors defined above in establishing Rules 1–4 we rewrite (3.51) as

$$\hat{\psi}_{sp}(\mathbf{r},t)=u_pF(\mathbf{r}-\mathbf{r}_p''-\mathbf{R}_s,0)\ , \tag{3.59}$$

where

$$u_p=\left[\prod_j B_{jp}\right]e^{i(\mathbf{K}_p\cdot\mathbf{r}-\Phi_p)} \tag{3.60}$$

and

$$\Phi_p=\sum_j\Phi_{jp}^{\omega}-\sum_j\Phi_{jp}^{\epsilon}-\Phi_p^{\iota}\ . \tag{3.61}$$

We have reintroduced the sum over j to remind the reader of the association of the phase factors with the separate parts of the recoil diagrams.

Rule 6. Having found the effective wave packets we proceed to the calculation of expectation values (3.30) and (3.31), which entails evaluating $M_{p_1p_2}(\mathbf{k})$ in the form of either (3.50) or (3.43).

For a Doppler-broadened gas we assume a Maxwell-Boltzmann distribution to write

$$A^*(\mathbf{q})A(\mathbf{q})=\frac{1}{(2\pi mk_BT/\hbar^2)^{1/2}}e^{-\mathbf{q}^2/(2mk_BT/\hbar^2)} \tag{3.62}$$

and reexpresses the last term in (3.43) as

$$\begin{aligned}f_{p_1p_2}&=\int d^3\mathbf{q}\,A^*(\mathbf{q})A(\mathbf{q})e^{-i\mathbf{q}\cdot(\mathbf{r}_{p_1}''-\mathbf{r}_{p_2}'')}\\&=e^{-(mk_BT/2\hbar^2)(\Delta r'')^2}\ .\end{aligned} \tag{3.63}$$

Rules 7 and 8. We combine the above factors to ex-

press $M_{p_1p_2}(k)$ in the form

$$U_{n_1n_2}=(2\pi)^3N\sum_{p_1}^{n_1}\sum_{p_2}^{n_2}u_{p_1}u_{p_2}^{*}f_{p_1p_2}(t) \tag{3.64}$$

which leads directly, via (3.30) and (3.31), to the population in state $|n\rangle$

$$\langle\langle N_n\rangle\rangle=U_{nn} \tag{3.65}$$

and the source of emission along $\mathbf{k}$ from $|n_1\rangle\rightarrow|n_2\rangle$

$$\langle\langle \mathbf{P}e^{-i\mathbf{k}\cdot\mathbf{r}}{}_{n_1n_2}\rangle\rangle=\mathbf{p}_{n_1n_2}U_{n_1n_2}\ , \tag{3.66}$$

where $\mathbf{p}_{n_1n_2}=\langle n_2|\mathbf{P}|n_1\rangle$.

IV. APPLICATIONS

In this section we wish to apply the billiard-ball theory to the analysis of three experiments involving the manipulation of matter-waves by laser light. The first involves the determination of the acceleration of gravity by the measurement of the excited-state population of a cooled gaseous medium after optical excitation, by a pair of standing-wave pulses, and a traveling-wave pulse [5]; the second the measurement of rotation using Ramsey fringes [6]; and the third the deflection of an atomic beam by a standing-wave laser beam [10]. This is in the inverse order according to which they appear in the literature. We treat the earliest work last because it relates to another work [12], earlier yet, performed in a gas and involving the delayed generation of a grating by a pair of standing-wave excitation pulses. The BB analysis of [5] and [6] is handled rather simply and so we deal with them first. The treatment of [10] and [12] is more involved. In particular, the BB analysis predicts an effect observed but not understood in [12].

A. Gravity measurement

The acceleration of gravity was measured by taking a gas of Na atoms, exciting them with a sequence of three equally spaced laser pulses and then probing the final excited-state population with a fourth pulse which resonantly ionized them [5]. The excitation pulses were directed in the vertical direction and the action of gravity was detected by a modulation in the ionization signal as the frequencies of the laser pulses were varied.

1. Experimental arrangement

Na atoms were loaded into an optomagnetic trap, cooled, launched, and then optically pumped into the $F=1$, $m_F=0$ ground hyperfine state. Following the launch a set of vertically directed, counterpropagating Raman laser beams was pulsed on three times to drive a $\pi/2-\pi-\pi/2$ pulse sequence. The Raman frequency was tuned to make transitions to the $F=2$, $m_F=0$ ground hyperfine state. The population of the $F=2$ state was detected by resonant ionization.

The Raman hyperfine transition was chosen to avoid spontaneous-emission limitations. The lasers were tuned near the $3S_{1/2}$-$3P_{3/2}$ transition frequency yet detuned enough so that the three-level system could be treated as an equivalent two-level system. For such a system the effective frequency of the exciting pulses is the laser modulation frequency, i.e., the Raman frequency. Since each pulse was formed by two counterpropagating components the effective wave vector was $\mathbf{k}_l=2\mathbf{k}$, where $k=2\pi/\lambda$ and λ is the optical wave length. The three pulses were, in addition, successively detuned; their phases were

$$\Phi_{1p}^{\varphi}=\mathbf{k}_l\cdot\mathbf{r}-\omega_0t-\varphi_1\ ,$$

$$\Phi_{2p}^{\varphi}=\mathbf{k}_l\cdot\mathbf{r}-(\omega_0+\omega_m)t-\varphi_2\ ,$$

$$\Phi_{3p}^{\varphi}=\mathbf{k}_l\cdot\mathbf{r}-(\omega_0+2\omega_m)t-\varphi_3\ .$$

This successive detuning of the Raman frequency generates the "Ramsey fringes" on varying its ω_m. As we shall see this depends on the phase difference $\Delta\varphi=\varphi_1-2\varphi_2+\varphi_3$ being held constant, as indeed it was. The pulses were equally spaced, i.e., $t_3-t_2=t_2-t_1=\tau$.

2. Recoil diagram

The recoil diagram for the process described above, cf. Fig. 5, is similar to that for the two-pulse echo, cf. Fig. 3, except that the coherence produced spontaneously at the echo time is transferred to a "population" coherence. The existence of Ramsey fringes is then determined by applying Rule 2,

$$\Phi_{p_1}^{\varphi}=(\mathbf{k}_l\cdot\mathbf{r}-\omega_0t_1-\varphi_1)-[\mathbf{k}_l\cdot\mathbf{r}-(\omega_0+\omega_m)t_2-\varphi_2]+[\mathbf{k}_l\cdot\mathbf{r}-(\omega_0+2\omega_m)t_3-\varphi_3]$$

and

$$\Phi_{p_2}^{\varphi}=+[\mathbf{k}_l\cdot\mathbf{r}-(\omega_0+\omega_m)t_2-\varphi_2]\ ,$$

which yields

$$\Delta\Phi_{p_1p_2}^{\varphi}=\Phi_{p_1}^{\varphi}-\Phi_{p_2}^{\varphi}=-2\omega_m\tau-\Delta\varphi\ .$$

Thus the Ramsey fringes are obtained as long as $\Delta\varphi$ is kept constant. (Although the excitation diagram here is the same as Fig. 5 and hence closes, Ramsey fringes are possible in violation of the usual rule because the several laser frequencies depend differently on ω_m.) The alternative diagram, cf. Fig. 4, does not generate fringes because the corresponding fixed phase $\varphi_3-\varphi_1$ is not held constant.

The sensitivity of this experiment to the action of gravity is determined by applying Rule 4: $\Delta\Phi_{p_1p_2}^{\iota}=(m/\hbar)\dot{\mathbf{v}}\cdot\mathbf{A}_{p_1p_2}$. Writing the acceleration of gravity as $\dot{\mathbf{v}}=-G\hat{\mathbf{z}}$ and taking from the recoil diagram $\mathbf{A}_{p_1p_2}=(\hbar/m)\mathbf{k}_l\tau^2$, we obtain

$$\Delta\Phi_{p_1p_2}^{\iota}=-\mathbf{k}_l\cdot\hat{\mathbf{z}}\mathbf{G}\tau^2\ ,$$

which is just the result of [5].

3. *Ramsey fringes*

We summarize by adding the phases from Rules 2 and 4

$$\Delta\Phi_{p_1p_2} = -\mathbf{k}_l\cdot\hat{\mathbf{z}}G\tau^2 - 2\omega_m\tau - \Delta\varphi \ ,$$

which show the essential features of the gravity experiment.

B. Rotation measurement

The angular velocity of a platform was measured by performing a Ramsey-fringe experiment using a Ca-atomic-beam apparatus mounted thereon [6]. Rotation was detected by measuring the shift in the Ramsey-fringe pattern when the direction of rotation was reversed.

1. *Experimental arrangement*

A dye laser was coupled to the apparatus by an optical fiber and divided into four parallel beams directed normal to the atomic beam. The plane defined by the atomic beam and the laser beams was horizontal and parallel to the surface of the platform. The platform was rotated about the vertical axis. The first two laser beams were copropagating and separated by an amount D was were the second two laser beams. The two pairs were counterpropagating and the separation between the second and third laser beams was d.

2. *Recoil diagram*

BB analysis leads to a recoil diagram, cf. Fig. 9, which is equivalent to Fig. 3 of [6]. In fact their Fig. 3 is intended to describe two interfering recoil trajectories. At t_1 and t_2 the laser beams are directed along $\mathbf{k}_+ = \mathbf{k}$ while at t_3 and t_4 they are directed along $\mathbf{k}_- = -\mathbf{k}$. We show the four paths which lead to the Doppler-free coherences in the excited-state populations. We ignore additional trajectories launched at t_3 and t_4 since they do not lead to any such coherences. The time between the first and second pulses is $\tau = D/v_\parallel$ as is the time between the third and fourth; $v_\parallel$ is the longitudinal velocity of the atom under consideration and D is the distance between the first and second and the third and fourth laser beams. The time between the second and third pulses is $T = d/v_\parallel$; d is the distance between the second and third atomic beams. For good results the beam is prepared so that $v_\parallel$ is concentrated near its average value. Otherwise the signal should be averaged over $v_\parallel$.

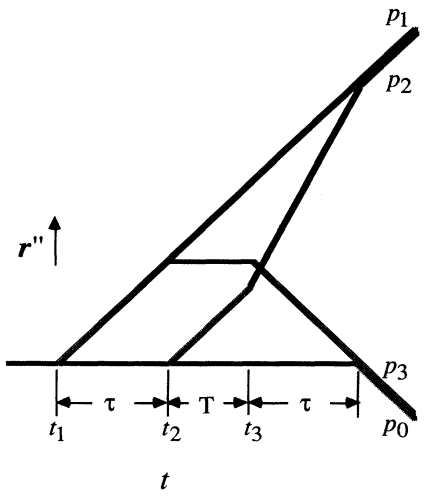

FIG. 9. Recoil ($\mathbf{r}''$ vs t) diagram for the rotation detector. Four laser pulses are applied at t_1, t_2, t_3, and t_4 separated by τ, T, and τ, respectively. Two coherent-state superpositions form at t_4. Rotation induces the phase shift proportional to the enclosed area in each diagram. Contributions from both diagrams are identical except for quadratic recoil phase.

3. *Ramsey fringes*

Ramsey fringes are identified with the excited-state population modulations resulting from sweeping the laser frequency. They arise because the successive laser pulses are phase coherent. Applying Rule 2 to paths p_0 and p_3 we get

$$\Phi^{\varphi}_{p_3} = +(\mathbf{k}_+\cdot\mathbf{r} - \omega t_1) - (\mathbf{k}_+\cdot\mathbf{r} - \omega t_2) + (\mathbf{k}_-\cdot\mathbf{r} - \omega t_3)$$

with

$$\Phi^{\varphi}_{p_0} = +(\mathbf{k}_-\cdot\mathbf{r} - \omega t_4)$$

so that

$$\Delta\Phi^{\varphi}_{p_0p_3} = -2\omega\tau \ .$$

We did not need to include the arbitrary phase factors φ since the laser beams come from a single source. The excited-state population is thus modulated by a full cycle each time the laser frequency is changed by π/τ.

4. *Quadratic recoil phase*

Application of Rule 3 for $\Phi^{K^2}p$ applied to paths p_0 and p_3 yields

$$\Phi^{K^2}_{p_3} = -\frac{\hbar}{2m}[\mathbf{k}_+^2(t_2 - t_1) + \mathbf{k}_-^2(t_4 - t_3)], \quad \Phi^{K^2}_{p_0} = 0$$

and therefore

$$\Delta\Phi^{K^2}_{p_0p_3} = \frac{\hbar}{2m}(2k^2\tau) \ .$$

This term also depends on $\omega = kc$ but it is negligible compared to $\Delta\Phi^{\omega}_{p_0p_3}$.

5. *Rotational phase*

The effect of the rotation is to introduce an overall phase which shifts the fringe pattern. This phase is given by the Φ^{ι}_{p} of (3.56). Its magnitude is obtained directly from Fig. 9. We find

$$\mathbf{A}_{p_3} = \frac{\hbar\mathbf{k}}{m}(t_2 - t_1)[\tfrac{1}{2}(t_2 - t_1) + (t_3 - t_2) + \tfrac{1}{2}(t_4 - t_3)]$$

$$= \frac{\hbar\mathbf{k}}{m}\tau(\tau + T)$$

and

$$\mathbf{A}_{p_0}=0 .$$

Rotation, at angular velocity $\boldsymbol{\Omega}_{\rm rot}$, of the platform on which the experiment is being carried out means that

$$\dot{\mathbf{Q}}=-\boldsymbol{\Omega}_{\rm rot}\times\mathbf{Q} ,$$

where $\mathbf{Q}=\mathbf{q}+\mathbf{q}_{\|}+\mathbf{q}'$ and $\hbar\mathbf{q}_{\|}=m\mathbf{v}_{\|}$ is essentially the classical momentum of the atom; see Appendix B. Thus $\mathbf{q}_{\|}$ is a c number and $\mathbf{q}$ is a quantum-mechanical fluctuation.

For the slow rotations with which we are concerned it is sufficient to write

$$\dot{\mathbf{q}}'\cong-\boldsymbol{\Omega}_{\rm rot}\times\mathbf{q}_{\|}$$

in which case

$$\Delta\Phi^{\iota}_{p_0p_3}=\dot{\mathbf{q}}\cdot\mathbf{A}_{p_0p_3}$$
$$=-(\boldsymbol{\Omega}_{\rm rot}\times\mathbf{v}_{\|})\cdot\mathbf{k}\tau(\tau+T) .$$

6. *Summary*

For $\boldsymbol{\Omega}_{\rm rot}$, $\mathbf{v}_{\|}$, and $\mathbf{k}$ mutually perpendicular we obtain

$$\Delta\Phi^{\varphi}_{p_0p_3}+\Delta\Phi^{K^2}_{p_0p_3}+\Delta\Phi^{\iota}_{p_0p_3}$$
$$=\left[-\omega+\frac{\hbar}{2mc^2}\omega^2+2\pi\Omega_{\rm rot}\frac{v_{\|}(\tau+T)}{\lambda}\right]2\tau .$$

If we calculate $\Delta\Phi_{p_2p_1}$ we obtain the above result except that the sign of $\Delta\Phi^{K^2}$ is reversed. We make connection with the formula (6) in [6] by noting that $v_{\|}\tau=D$, $v_{\|}T=d$.

C. Diffraction of matter waves

The diffraction of atoms by light has been observed in an atomic beam of sodium atoms [10]. In that experiment the atomic beam passes through a near-resonant standing-wave laser beam which is directed normal to the atomic beam. The atoms are thus subject to a pulse of standing-wave light from which they recoil according to the number of photons they are induced to absorb and the number they are stimulated to emit. The BB analysis applied to this problem parallels the analysis of Gould, Ruff, and Pritchard [10]. The action of the standing-wave light pulse is to generate the fan like structure starting at t_1 (the time the pulse is applied) as shown in the recoil diagram of Fig. 10. The momentum of each trajectory is indicated on the diagram. These trajectories are real as was demonstrated in [10] by their spatial differentiation downstream of the laser beam. They continue indefinitely beyond the area of the figure. (In connection with [10] one should disregard the second fan at t_2.)

This analysis recalls a related experiment performed earlier in which two successive standing-wave light beam pulses were directed into a gas of sodium atoms followed by a third traveling wave whose purpose was to probe the formation of an atomic grating [12]. The immediate

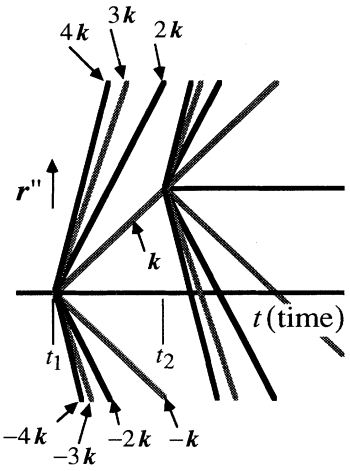

FIG. 10. Recoil (r'' vs t) diagram for standing-wave excitations I. The standard wave pulse at t_1 generates a local atomic grating and discrete momentum distribution which in an atomic beam results in a large spatial atomic separation downstream of the laser beam. The fanlike structure shows the wave packets splitting and separating. Application of a second standing-wave pulse at t_2 produces additional fanlike structures (we only show one).

effect of the first standing-wave pulse is to generate a real atomic grating with spacing $\lambda/2$, where λ is the optical wavelength. This grating washes out quickly because of the spread in initial transverse velocities, but is reformed in an echolike manner after a second standing-wave pulse. The reformed grating is probed by a third traveling-wave pulse.

The two experiments just described are like two complementary ways of revealing an optical diffraction grating. Either light emerging from the grating can be allowed to form a diffraction pattern dual to the grating itself—this is what the atoms do in [10]—or this same light can be refocused to form an image of the original grating, as the atoms are refocused in [12]. The second standing wave in [12] plays the part of the imaging lens.

In [12] the spread of initial momenta $\mathbf{q}$ of the atoms is much larger than $\mathbf{k}$, but in [10] it is much smaller, in the direction transverse to the atomic beam. This corresponds to the fact that light must emerge coherently from a grating in order to form a diffraction pattern, but it can be reformed into an image of the grating even if it is incoherent. Thus in [10] the billiard balls must be elongated transversely over many wavelengths. Nevertheless the first part of the recoil diagram of Fig. 10 makes sense if the trajectories are extended until they fall outside the original atomic beam, for then even the elongated billiard balls are well separated.

1. *Effect of a second standing-wave pulse*

In [12], however, the billiard balls can be regarded as small. In Fig. 10 we see the recoil diagram which results from the application of two successive standing-wave

pulses at t_1 and at $t_2=t_1+\tau$. On each trajectory there appears, at the time of the second pulse, the same fanlike pattern. We show here only one such fan and we label the trajectories, which extend indefinitely. The complete recoil diagram is very cluttered when standing-wave fields are applied, cf. Fig. 11, where we have shown only two fans at the time of the second pulse. The complications notwithstanding, there is considerable enlightenment to be obtained by their perusal. For example we see a multitude of trajectory crossings indicating the existence of multiple coherences. Whenever two trajectories associated with the same electronic state cross it means that a population grating has been formed. Seven such gratings are identified by the circles in Fig. 11 occurring at $t_2+\frac{1}{2}\tau$. These are characterized by a wave vector $2\mathbf{k}$, where $\mathbf{k}$ is the wave vector associated with both the standing waves, i.e., they have the same periodicity as the standing-wave light pulse. There are eight other gratings displayed in this figure but they are associated with a different wave vector and not pertinent to our analysis.

The periodic array of circles in Fig. 11 must not be mistaken for a picture of a grating, even though the vertical coordinate does represent distance. The grating has spacing $\frac{1}{2}\lambda=\pi/k$, whereas the circles are spaced at $(\hbar k/m)(t_2-t_1)/2$. Nor does the vertical displacement of the circles represent relative displacement of different gratings. The recoil diagram is not a complete picture of atomic displacement but only displays the vectors $\mathbf{r}''_{p_1},\mathbf{r}''_{p_2}$ that enter into (3.43) and (3.52). To extract the grating from those equations, one may note that the Fourier transform at $2\mathbf{k}$ of the ith state density is given by $\sum^i_{p_1}\sum^i_{p_2}M_{p_1p_2}(2\mathbf{k})$. Evidently, from (3.52), $\mathbf{r}''_{p_1}$ and $\mathbf{r}''_{p_2}$ must coincide in order to make a strong grating, but they do not enter into the phase $\Delta\Phi$ which would govern displacement of the grating. In fact, $\Delta\Phi^{\varphi}_{p_1p_2}$ is the same for all the crossings marked by the circles in Fig. 11; $\Delta\Phi^{\iota}_{p_1p_2}$ is zero (no external field) and $\Delta\Phi^{\epsilon}_{p_1p_2}$ is very small. The different circles, then, contribute *incoherently,* (i.e., by addition of M, not of ψ) to the *same* grating (same $\Delta\Phi$).

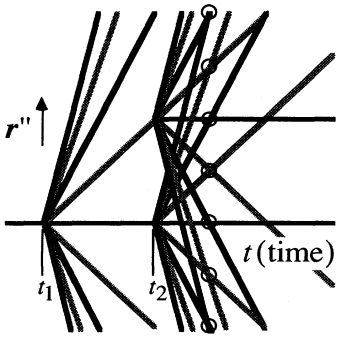

FIG. 11. Recoil ($\mathbf{r}''$ vs t) diagram for standing-wave excitations II. Same as Fig. 9 except that an additional fanlike structure at t_2 is shown. The crossings at $t_2+\tau/2$ (corresponding to population-grating formation) are marked by circles.

2. *Backscattering*

The object of the experiment in [12] was to detect the gratings circled in Fig. 11. This was accomplished by probing the gas with a pulse and looking for the backscattered signal. The experiment was successful, but it was noted that the backscattered signal was maximized when the third pulse was applied ≈ 2 ns *before* $t_2+\frac{1}{2}\tau$. The laser pulses were 3.5 ns in duration and the spacing of the standing-wave pulses was of the order of 20 ns. Thus the effect was subtle.

3. *Subtle effect*

This effect can be explained by means of recoil diagram with one crossing isolated for reasons of clarity, cf. Fig. 12. Here we show the grating being reformed in the ground state. The application of a pulse at t_3 *before* $t_2+\frac{1}{2}\tau$ produces the excited-state trajectory with wave vector $\mathbf{K}=\mathbf{k}_1-3\mathbf{k}_2+\mathbf{k}_3=-\mathbf{k}$ when all beams are colinear. Thus its crossing with the trajectory $\mathbf{K}=0$ produces a photon echo *after* $t_2+\frac{1}{2}\tau$ which radiates along $-\mathbf{k}$, i.e., in the backward direction. When $t_3=t_2+\frac{1}{2}\tau$ the echo signal is prompt, showing that it arises from backscattering from a grating. For $t_3>t_2+\frac{1}{2}\tau$ there is no crossing and no signal is expected. The analysis of [12] was confined to the actual grating and so predicted a backscattered signal only at $t_3=t_2+\frac{1}{2}\tau$. But Fig. 12 shows that a similar signal should appear for $t_3=t_2+\frac{1}{2}\tau-\Delta t$. The question is why Δt was found to extend only to about 5 ns (maximum effect at 2 ns).

4. *Relaxation*

The answer to this question has to do with the spontaneous lifetime of the excited state which in Na is 16 ns. The standing-wave pulse separation times are already greater than 20 ns which means that we can neglect the contribution of backscattering from the excited-state gratings. As seen from the recoil diagram, if $t_3=t_2+\frac{1}{2}\tau-\Delta t$, the atom stays in the excited state an extra time $\approx 2\Delta t$. For $\Delta t=5$ ns this cuts down the signal

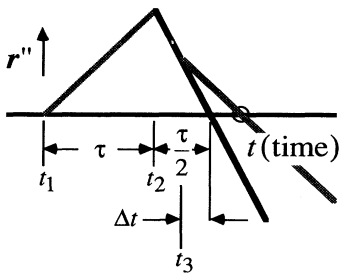

FIG. 12. Recoil ($\mathbf{r}''$ vs t) diagram for standing wave III. A third pulse with wave vector $\mathbf{k}$ is applied at t_3 to study the crossings (one suffices) circled in Fig. 10. When Δt is positive there is a delayed crossing of the resulting excited-ground-state superposition which has a wave vector $-\mathbf{k}$. This means that echolike radiation should appear in the backward direction. It is prompt (signifying backscattering off a grating) when $\Delta t=0$.

by $\approx 50\%$. But for $t_3 = t_2 + \frac{1}{2}\tau + \Delta t$ the signal disappears as soon as Δt exceeds the pulse duration 3.5 ns. This asymmetry in Δt is the *subtle* effect referred to in [12].

V. TWO WAYS TO SKIN A CAT

In echolike experiments designed to detect external force fields, the signal arises from the term $(\hbar^2/m)\mathbf{K}\cdot\mathbf{Q}$ in the kinetic energy, where $\hbar(\mathbf{Q}+\mathbf{K})$ is the total atomic momentum, $\mathbf{K}$ being that part due to interaction with the laser light.

We previously chose to express the factor $(\hbar/m)\mathbf{K} = d\mathbf{r}''/dt$ as a recoil *velocity*. Thus we have rewritten the phase $\Phi^{\iota} = \int (\hbar/m)\mathbf{K}\cdot\mathbf{Q}dt$ as $-\int \mathbf{Q}\cdot d\mathbf{r}''$ and through an integration by parts arrived at Rule 4 containing the term $\dot{\mathbf{Q}}\cdot\mathbf{A}$. The factor $\mathbf{A}$ is then read graphically as the area in the recoil diagram, while the factor $\dot{\mathbf{Q}}$ is applied abstractly.

Alternatively we could read $(\hbar/m)\mathbf{Q} = d\mathbf{R}/dt$ as the *recoil-free* atomic velocity, in which case $\Phi^{\iota} = -\int \mathbf{K}\cdot d\mathbf{R}$, where $\mathbf{R}$ is the position the atom would have classically in the absence of the pulses. Then an integration by parts (in the opposite sense from before) would lead to a term $\int \mathbf{R}\cdot d\mathbf{K} = \sum_j \tilde{\mathbf{k}}_j \cdot \mathbf{R}_j$ since $\mathbf{K}$ changes only at the pulse times. In this term the factor $\mathbf{R}$ can be read graphically from a drawing of the recoil-free trajectory, while the factor $\mathbf{k}$ is abstract. Note that the roles of $\mathbf{K}$ and $\mathbf{Q}$ are reversed.

This "recoil-free trajectory" (RFT) picture leads to a curved path—cf. Fig. 13 where it is applied to the gravity experiment of Kasevich and Chu [5]—instead of the segmented straight-line paths of the billiard-ball model, cf. Fig. 5.

The RFT picture is separated from the BB picture by *two* integrations by parts. The two pictures are complementary and should not be confused. In the RFT picture one draws a single curved trajectory without recoil and multiplies each $\mathbf{R}_j$ by the nongraphical factor $\tilde{\mathbf{k}}_j$. In the BB picture one compares a pair of straight-line trajectories and multiplies the enclosed area by the nongraphical $\dot{\mathbf{q}}'$.

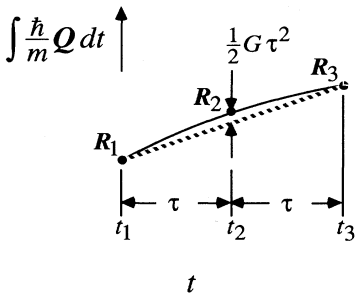

FIG. 13. Parabolic path [$\int (\hbar/m)\mathbf{Q}\,dt$ vs t] associated with the RFT picture. The atomic path is graphed as a function of time neglecting recoil due to photon absorption and emission. The curvature is due to gravity. The relative phase factor arising from recoil is

$$\exp\left[i\sum_{j=1}^{3}\left[\tilde{\mathbf{k}}_{\iota_{jp_1}} - \tilde{\mathbf{k}}_{\iota_{jp_2}}\right]\cdot\mathbf{R}_j\right] = e^{i\mathbf{k}_{\iota}\cdot(\mathbf{R}_1 - 2\mathbf{R}_2 + \mathbf{R}_3)}.$$

If $t_2 - t_1 = t_3 - t_2 = \tau$ (echo condition) then since $\mathbf{R}_j = \mathbf{v}_0 t_j + \frac{1}{2}\dot{\mathbf{v}}(t_j - t_1)^2$ the phase factor is the same for all initial velocities $\mathbf{v}_0$, namely $e^{-iG\tau^2 k}$ if $\mathbf{k}_{\iota}$ is directed upward, in agreement with Rule 4 applied to Fig. 5.

The computation of Kasevich and Chu [5] corresponds to the RFT picture, although the trajectories shown in Fig. 1(a) give the appearance of a recoil diagram. Riehle *et al.* display both calculations following their Eq. (1) [6]. Their rules (1), (2), (3) are the same as our Rules 3, 2, 4 in the BB picture. Their second point of view, Eq. (5) ff, is that of the RFT picture.

Note added in proof. The BBM analysis has been applied [21] to echo generation by optical standing-wave pulses to obtain enhanced sensitivity to external and acceleration fields. It has also been used [22] to analyze echo modulation in a gas of molecules whose vibrational modes are displaced by electronic excitation.

ACKNOWLEDGMENTS

This work is supported by the U.S. office of Naval Research (S.R.H.) and the U.S. DOE (R.F.).

APPENDIX A: SINGLE-ATOM ECHO

The standard echo experiment simply detects a radiated signal of coherent intensity ($\approx N^2$) at the echo time. The amplitude of the signal depends on the expectation value of a dipole moment operator which is coherently reconstituted at that time.

In such an experiment there must be many atoms present at the same time, since the factor N^2 can arise only from constructive interference among atoms. This interference requires that it not be possible to determine which of many atoms emitted the echo. In a repeated experiment on one atom, it would be manifest that an echo photon was emitted on some occasions and not on others, so that the interference would be absent.

There are, however, certain modifications by which a single-atom echo can be displayed in a signal accumulated over repeated experiments. One is homodyne detection, in which one measures not the intensity of the echo but its polarization amplitude, by interfering it with a light beam coherently related to the pulses causing the echo. Here the detector cannot tell whether a photon belongs to the echo or to the reference beam. Hence, in repeated experiments on one atom, it cannot tell which experiments yielded an echo photon, and so interference between different experiments is possible.

Another such modification is the use of a probe pulse at the echo time. One then measures the coherently reconstituted dipole moment not by its radiated field but by converting the associated off-diagonal density-matrix element (transverse Bloch vector component) into a diagonal element (longitudinal component) which shows up as an atomic population difference. This technique is used, for example, in both [6] and [5]. Here again, since the signal appears as a statistical effect on populations, there is no way to tell which atoms were converted to the excited state by the probe pulse and which were already in

that state. Thus interference is possible between two histories, and remains possible if the experiment is done repeatedly on a single atom, since the history on each occasion is not detectable.

APPENDIX B: ATOMIC BEAMS

Our analysis has been tailored to a gas—that is, an assemblage of atoms homogeneous in space (x,y,z) and evolving in time (t). But it is easily adapted to an atomic beam—that is, an assemblage homogeneous in (t) and in (x,y) and evolving in the longitudinal direction z. In a gas, laser pulses are applied at certain times t_j; in the atomic beam; laser cw beams are encountered at certain positions z_j. In a beam the momenta $\hbar\mathbf{q}$ are augmented by a fixed $\hbar\mathbf{q}_\parallel = mv_\parallel\hat{\mathbf{z}}$.

Most simply, one may regard $z = v_\parallel t$ as a classical variable, for an atom with longitudinal velocity $v_\parallel$. Then the collimated cw laser beams are felt by the atom as short pulses. The analysis goes through as before, except that $d^3\mathbf{r}$ should be replaced by $d^2\mathbf{r} = dx\,dy$. The atomic beam must be many wavelengths wide in order to sustain the $\mathbf{q}$ conservation represented in (3.34). This "width," however, can just as well be the statistical dispersion of atoms shot one at a time.

It may be objected that this treatment assumes that each atom emerges from the source at a definite time, whereas in atomic-beam experiments the time may be known to less accuracy than the duration of flight, and the atomic wave function may well be spread longitudinally through the apparatus so that the laser beams do not act as short pulses. Perhaps one should treat the atoms as if in stationary states so that the temporal uncertainty is infinite.

Accordingly, one may proceed as follows. Write the Hamiltonian of the atom as

$$H = H_{\text{long}} + H_{\text{trans}} + H_{\text{force}} + H_{\text{int}} + H_{\text{rad}} , \tag{B1}$$

where

$$H_{\text{long}} = -\frac{\hbar^2}{2m}\frac{\partial^2}{\partial z^2} , \tag{B2}$$

$$H_{\text{trans}} = -\frac{\hbar^2}{2m}\left[\frac{\partial^2}{\partial x^2} + \frac{\partial^2}{\partial y^2}\right] , \tag{B3}$$

$$H_{\text{int}} = \begin{bmatrix} 0 & 0 \\ 0 & \hbar\omega_0 \end{bmatrix} , \tag{B4}$$

$$H_{\text{rad}} = \begin{bmatrix} 0 & \sum_j f_j(z)^* e^{-i\mathbf{k}_j\cdot\mathbf{r}} e^{i\omega t} \\ \sum_j f_j(z) e^{i\mathbf{k}_j\cdot\mathbf{r}} e^{-i\omega t} & 0 \end{bmatrix} , \tag{B5}$$

and H_{force} commutes with H_{long}. (If H_{force} is the Coriolis effect this is true to first order in the angular velocity Ω_{rot} of the collimated beam.) In H_{rad} we have dropped counterrotating terms; $f_j(z)$ defines the collimation of the jth laser beam, and the $\mathbf{k}_j$ are all $\perp\hat{z}$; all lasers have the same frequency ω.

We now write the wave function of an atom as

$$\psi(\mathbf{r},t) = \begin{bmatrix} 1 & 0 \\ 0 & e^{-i\omega t} \end{bmatrix}\bar{\psi}(\mathbf{r},t) . \tag{B6}$$

Schrödinger's equation then becomes $i\hbar\dot{\bar{\psi}} = \bar{H}\bar{\psi}$, where

$$\bar{H} = H_{\text{long}} + H_{\text{trans}} + H_{\text{force}} + \begin{bmatrix} 0 & \sum_j f_j(z)^* e^{-i\mathbf{k}_j\cdot\mathbf{r}} \\ \sum_j f_j(z) e^{i\mathbf{k}_j\cdot\mathbf{r}} & \hbar(\omega_0-\omega) \end{bmatrix} . \tag{B7}$$

Since $\bar{H}$ is time independent, we can assume that $\bar{\psi}$ is "stationary" with eigenvalues $E_\parallel = \frac{1}{2}mv_\parallel^2$. Then we write

$$\bar{\psi}(\mathbf{r},t) = e^{-iE_\parallel t} e^{iq_\parallel z}\bar{\bar{\psi}}(\mathbf{r}) \tag{B8}$$

and $\bar{\bar{\psi}}(\mathbf{r})$ satisfies

$$\left[\frac{\hbar^2}{2m}\left[q_\parallel - i\frac{\partial}{\partial z}\right]^2 - \frac{\hbar^2}{2m}q_\parallel^2 + H_{\text{trans}} + H_{\text{force}} + \begin{bmatrix} 0 & \sum_j f_j(z)^* e^{-i\mathbf{k}_j\cdot\mathbf{r}} \\ \sum_j f_j(z) e^{i\mathbf{k}_j\cdot\mathbf{r}} & \hbar(\omega_0-\omega) \end{bmatrix}\right]\bar{\bar{\psi}} = 0 \tag{B9}$$

or

$$-i\hbar v_{\parallel}\frac{\partial}{\partial z}\bar{\bar{\psi}}=\left[H_{\text{trans}}+H_{\text{force}}+\begin{bmatrix}0 & \sum_j f_j(z)^* e^{-i\mathbf{k}_j\cdot\mathbf{r}}\\ \sum_j f_j(z)e^{i\mathbf{k}_j\cdot\mathbf{r}} & \hbar(\omega_0-\omega)\end{bmatrix}+\frac{\hbar^2}{2m}\frac{\partial^2}{\partial z^2}\right]\bar{\bar{\psi}} \tag{B10}$$

from which the term in $\partial^2/\partial z^2$ can be dropped since the laser collimation width is much greater than $q_{\parallel}^{-1}$. This gives us a pseudo-Schrödinger equation with $z/v_{\parallel}$ playing the role of time. In this framework the functions $f_j(z)$ define short pulses. The previous analysis goes through.

It should be borne in mind that the time between "pulses" depends on $v_{\parallel}$, and if the atoms are not narrowly velocity selected there is a possibility of smearing out any signal whose phase depends on this time. But in the absence of any force field this just leads to the well-known decay of Ramsey fringes at large detuning. The quadratic recoil phase $\int(\hbar/2m)\mathbf{k}^2dt$ will, if not negligible, only shift the central maximum. As for the force field, if it is due to rotation then H_{force} is also proportional to $v_{\parallel}$ and its effect on $\partial/\partial z\bar{\bar{\psi}}$ in (B10) is $v_{\parallel}$ independent. [This appears in (3.56) where $\mathbf{A}=\int\mathbf{r}''dz/v_{\parallel}$ and $\dot{q}'=-\boldsymbol{\Omega}_{\text{rot}}\times\mathbf{q}_{\parallel}=-\boldsymbol{\Omega}_{\text{rot}}\times\hat{\mathbf{z}}mv_{\parallel}/\hbar$. More elegantly, one may transfer the Coriolis factor $v_{\parallel}$ from $\dot{\mathbf{q}}$ to $\mathbf{A}$ so that $\mathbf{A}$ becomes a true area $\int\mathbf{r}''dz$, as done in [6].)

APPENDIX C: ACTION OF A PULSE

To follow the effect of an incident pulse (the nth in a sequence) on the system, assume that the pulse consists of a strong field

$$\mathbf{E}=\text{Re}(E_0\hat{\epsilon}e^{i(\mathbf{k}\cdot\mathbf{r}-\omega t)}), \tag{C1}$$

acting for a short time τ. We treat the field classically, as is usual in discussing Rabi precession, and assume that the additional field produced by the atoms themselves is negligible; the system is optical thin. Then the fields acts separately on each atom. We assume that E_0 is constant in amplitude during τ.

Consider the sth atom. Its internal states are labeled as $|i\rangle$. Its Hamiltonian is

$$H=H_{\text{kin}}+H_{\text{self}}+H_{\text{int}}, \tag{C2}$$

where

$$H_{\text{kin}}=-\frac{\hbar^2}{2m}\nabla^2, \tag{C3}$$

$$H_{\text{self}}=\sum_i|i\rangle\hbar\Omega_i\langle i|, \tag{C4}$$

and

$$H_{\text{int}}=-\sum_{i,j}P_{ij}\text{Re}\left[E_0e^{i(\mathbf{k}\cdot\mathbf{r}-\omega t)}\right]|i\rangle\langle j| \tag{C5}$$

where

$$P_{ij}=\langle i|\mathbf{P}\cdot\hat{\epsilon}|j\rangle, \tag{C6}$$

$\mathbf{P}$ being the atomic dipole moment operator. The term H_{int} acts only during the time τ.

1. Neglecting H_{kin} during τ

We assume that τ is so short that H_{kin} has no effect during the pulse. We also assume that each pair of states is either clearly on resonance ($||\Omega_i-\Omega_j|-\omega|\ll\tau^{-1}$) or far-off resonance ($||\Omega_i-\Omega_j|-\omega|\gg\tau^{-1}$) and that the matrix elements of H_{int} between off-resonant pairs can be disregarded because of fast oscillation [20]. For the same reason we shall drop the counterotating part of $\mathbf{E}$ in the resonant transitions.

For simplicity we also suppose that there are no multiphoton or cascade resonances. Then the internal Hilbert space of the atom decomposes into (a) one-dimensional blocks in which

$$H_{\text{self}}+H_{\text{int}}=H_{\text{self}}=\hbar\Omega_i \tag{C7}$$

and (b) two-dimensional blocks in which

$$H_{\text{self}}+H_{\text{int}}=\begin{bmatrix}\Omega_l & \frac{1}{2}P_{lu}E_0^*e^{-i\mathbf{k}\cdot\mathbf{r}}e^{i\omega t}\\ \frac{1}{2}P_{ul}E_0e^{i\mathbf{k}\cdot\mathbf{r}}e^{-i\omega t} & \Omega_u\end{bmatrix}, \tag{C8}$$

where $|i\rangle$ is a state not resonant with any other and $|l\rangle,|u\rangle$ are the lower and upper members of a resonant pair.

We introduce the rotating frame by defining the unitary operator $U_{\text{rot}}(t)$,

$$U_{\text{rot}}(t)=\begin{bmatrix}1 & \\ & e^{(1/2)i\omega t}\end{bmatrix}\text{ on one-dimensional blocks}$$
$$\begin{bmatrix}0 & \\ & e^{-(1/2)i\omega t}\end{bmatrix}\text{ on two-dimensional blocks.} \tag{C9}$$

Then if the wave function is expressed as

$$\Psi_s(t)=U_{\text{rot}}(t)\Psi_s'(t), \tag{C10}$$

Schrödinger's equation during the pulse takes the form

$$\begin{aligned}i\hbar\frac{d}{dt}\Psi_s'&=U_{\text{rot}}^{\dagger}(t)(H_{\text{self}}+H_{\text{int}})U_{\text{rot}}(t)\Psi_s'\\&\quad-i\hbar U_{\text{rot}}^{\dagger}(t)\dot{U}_{\text{rot}}(t)\Psi_s',\\&=H'\Psi_s',\end{aligned} \tag{C11}$$

where

$$H'=U_{\rm rot}^{\dagger}\left[H_{\rm self}+H_{\rm int}-i\hbar\frac{d}{dt}\right]U_{\rm rot}$$
$$=\begin{bmatrix}\hbar(\Omega_l+\frac{1}{2}\omega) & \frac{1}{2}P_{lu}E_0^{*}e^{-i\mathbf{k}\cdot\mathbf{r}}\\ \frac{1}{2}P_{ul}E_0e^{i\mathbf{k}\cdot\mathbf{r}} & \hbar(\Omega_u-\frac{1}{2}\omega)\end{bmatrix} \tag{C12}$$

in the two-dimensional blocks, and $H'=H_{\rm self}$ in the one-dimensional blocks.

Since H' is time independent, the transformation of Ψ_s' during the pulse is given by

$$U'=e^{-iH'\tau/\hbar}\,. \tag{C13}$$

In the one-dimensional blocks this is just $e^{-i\Omega_i\tau}$. In the two-dimensional blocks, we put $\omega=\Omega_u-\Omega_l$ by previous assumption so that

$$H'=\begin{bmatrix}\frac{\hbar}{2}(\Omega_l+\Omega_u) & \frac{1}{2}\hbar\omega_R e^{i\varphi}e^{-i\mathbf{k}\cdot\mathbf{r}}\\ \frac{1}{2}\hbar\omega_R e^{-i\varphi}e^{i\mathbf{k}\cdot\mathbf{r}} & \frac{\hbar}{2}(\Omega_l+\Omega_u)\end{bmatrix}$$
$$=\frac{\hbar}{2}(\Omega_l+\Omega_u)+\hbar\omega_R[\sigma_1\cos(\mathbf{k}\cdot\mathbf{r}-\varphi)+\sigma_2\sin(\mathbf{k}\cdot\mathbf{r}-\varphi)]\,, \tag{C14}$$

where σ_1, σ_2, and σ_3 are the Pauli matrices, and $\hbar\omega_R e^{-i\varphi}=P_{ul}E_0$ and $\hbar\omega_R e^{i\varphi}=P_{lu}E_0$. The quantity ω_R is the Rabi frequency.

If we now define

$$\sigma_R=\sigma_1\cos(\mathbf{k}\cdot\mathbf{r}-\varphi)+\sigma_2\sin(\mathbf{k}\cdot\mathbf{r}-\varphi)\,,$$
$$\sigma_R^2=1,\quad H'=\frac{\hbar}{2}(\Omega_1+\Omega_u)+\tfrac{1}{2}\hbar\omega_R\sigma_R\,, \tag{C15}$$

we have

$$e^{-(i/2)\omega_R\sigma_R\tau}=\cos(\tfrac{1}{2}\omega_R\tau)-i\sigma_R\sin(\tfrac{1}{2}\omega_R\tau) \tag{C16}$$

and so

$$U'=e^{-i(\Omega_l+\Omega_u)\tau/2}(\cos\tfrac{1}{2}\theta-i\sigma_R\sin\tfrac{1}{2}\theta)\,, \tag{C17}$$

where $\theta=\omega_R\tau$ is the pulse area.

Letting the pulse last from t_n to $t_n+\tau$, we find that Ψ_s is transformed by

$$U=U_{\rm rot}(t_n+\tau)U'U_{\rm rot}^{\dagger}(t_n)$$

$$=\begin{cases}e^{-i\Omega\tau}\ \text{on one dimensional blocks}\\[2ex]\begin{bmatrix}e^{-i\Omega_l(t_n+\tau)} & 0\\ 0 & e^{-i\Omega_u(t_n+\tau)}\end{bmatrix}\begin{bmatrix}\cos\frac{1}{2}\theta & -i\sin\frac{1}{2}\theta e^{-i(\mathbf{k}\cdot\mathbf{r}-\varphi)}\\ -i\sin\frac{1}{2}\theta e^{+i(\mathbf{k}\cdot\mathbf{r}-\varphi)} & \cos\frac{1}{2}\theta\end{bmatrix} & \text{(C18)}\\[2ex]\times\begin{bmatrix}e^{+i\Omega_l t_n} & 0\\ 0 & e^{+i\Omega_u t_n}\end{bmatrix}\ \text{on two-dimensional blocks}\,, & \text{(C19)}\end{cases}$$

where we have again replaced ω by $\Omega_u-\Omega_l$ and written $e^{-(1/2)i(\Omega_l+\Omega_u)\tau}$ as $e^{-(1/2)i(\Omega_l+\Omega_u)(t+\tau)}e^{+(1/2)i(\Omega_l+\Omega_u)t}$. In all this work $\mathbf{r}$ has been carried along as an operator that can act on the external wave function of the atom.

2. Respecting $H_{\rm kin}$ before τ

We now suppose that in the time interval before the nth pulse the atomic wave function of the atom took the form

$$\Psi_s=\sum_i\psi_{si}(\mathbf{r},t)|i\rangle+\sum_l\psi_{sl}(\mathbf{r},t)|l\rangle+\sum_u\psi_{su}(\mathbf{r},t)|u\rangle\,, \tag{C20}$$

where i ranges over the nonresonant states, l over the lower members of resonant pairs, and u over upper members of resonant pairs. We may write (μ standing for i, l, or u)

$$\psi_{s\mu}(\mathbf{r},t)=\sum_{\mathbf{q}}C_{\mu\mathbf{q}}e^{i\mathbf{q}\cdot\mathbf{r}}e^{-i[\Omega_\mu+(\hbar/2m)\mathbf{q}^2]t}\,. \tag{C21}$$

Let us designate by l' the upper partner of the lower resonant state l, and by u' the lower partner of the upper resonant state u. (Thus u,l' may designate the same state, but will refer to different histories.) Then by (C18)-(C21) we have the following.

3. Neglecting $H_{\rm kin}$ during τ

We have

$$\begin{aligned}\Psi_s(t_n+\tau)&=U\Psi_s(t_n)\\&=\sum_i|i\rangle\sum_{\mathbf{q}}C_{i\mathbf{q}}e^{i\mathbf{q}\cdot\mathbf{r}}e^{-i\Omega_i(t_n+\tau)}e^{-i(\hbar/2m)\mathbf{q}^2t_n}\\&\quad+\sum_l\sum_{\mathbf{q}}C_{l\mathbf{q}}e^{i\mathbf{q}\cdot\mathbf{r}}e^{-i(\hbar/2m)\mathbf{q}^2t_n}(|l\rangle\cos\theta e^{-i\Omega_l(t_n+\tau)}-|l'\rangle i\sin\theta e^{i(\mathbf{k}\cdot\mathbf{r}-\varphi)}e^{-i\Omega_{l'}(t_n+\tau)})\\&\quad+\sum_u\sum_q C_{u\mathbf{q}}e^{i\mathbf{q}\cdot\mathbf{r}}e^{-i(\hbar/2m)\mathbf{q}^2t_n}(|u\rangle\cos\theta e^{-i\Omega_u(t_n+\tau)}-|u'\rangle i\sin\theta e^{-i(\mathbf{k}\cdot\mathbf{r}-\varphi)}e^{-i\Omega_{u'}(t_n+\tau)})\,.\end{aligned}\tag{C22}$$

4. Respecting $H_{\rm kin}$ after τ

Now the expressions $e^{i\mathbf{k}\cdot\mathbf{r}}$ and $e^{-i\mathbf{k}\cdot\mathbf{r}}$ are operators acting on the external wave function to change its momentum; but since we are writing the wave function in position space these exponentials simply enter as factors. The subsequent application of the operator ∇^2 from $H_{\rm kin}$ will now produce factors $(\mathbf{q}\pm\mathbf{k})^2$ instead of $\mathbf{q}^2$. Hence after the application of the pulse we shall have

$$\begin{aligned}\psi_s(t)&=\sum_i|i\rangle\sum_{\mathbf{q}}C_{i\mathbf{q}}e^{i\mathbf{q}\cdot\mathbf{r}}e^{-i(\hbar/2m)\mathbf{q}^2(t-\tau)}e^{-i\Omega_it}\\&\quad+\sum_l\Bigg[|l\rangle\cos\theta\sum_{\mathbf{q}}C_{l\mathbf{q}}e^{i\mathbf{q}\cdot\mathbf{r}}e^{-i(\hbar/2m)\mathbf{q}^2(t-\tau)}e^{-i\Omega_lt}\\&\qquad-|l'\rangle i\sin\theta\sum_{\mathbf{q}}C_{l\mathbf{q}}e^{i(\mathbf{q}+\mathbf{k})\cdot\mathbf{r}}e^{-i\varphi}e^{-i(\hbar/2m)\mathbf{q}^2t_n}e^{-i(\hbar/2m)(\mathbf{q}+\mathbf{k})^2(t-t_n-\tau)}e^{-i\Omega_{l'}t}\Bigg]\\&\quad+\sum_u\Bigg[|u\rangle\cos\theta\sum_{\mathbf{q}}C_{u\mathbf{q}}e^{i\mathbf{q}\cdot\mathbf{r}}e^{-i(\hbar/2m)\mathbf{q}^2(t-\tau)}e^{-i\Omega_ut}\\&\qquad-|u''\rangle i\sin\theta\sum_{\mathbf{q}}C_{u\mathbf{q}}e^{i(\mathbf{q}-\mathbf{k})\cdot\mathbf{r}}e^{i\varphi}e^{-i(\hbar/2m)\mathbf{q}^2t_n}e^{-i(\hbar/2m)(\mathbf{q}-\mathbf{k})^2(t-t_n-\tau)}e^{-i\Omega_{u'}t}\Bigg]\,.\end{aligned}\tag{C23}$$

5. Setting τ to zero

But because we have neglected the action of $H_{\rm kin}$ during τ, we may as well throw away all terms $(\hbar/2m)\mathbf{q}^2\tau$, etc., in the exponents, obtaining

$$\begin{aligned}\psi_s(t)&=\Bigg[\sum_{\mu=i}+\cos\theta\sum_{\mu=l,u}\Bigg]|\mu\rangle\sum_{\mathbf{q}}C_{\mu\mathbf{q}}e^{i\mathbf{q}\cdot\mathbf{r}}e^{-i[(\hbar/2m)\mathbf{q}^2+\Omega_\mu]t}\\&\quad-i\sin\theta\Bigg[\sum_l e^{-i\varphi}|l'\rangle\sum_{\mathbf{q}}C_{l\mathbf{q}}e^{i(\mathbf{q}+\mathbf{k})\cdot\mathbf{r}}e^{-i[(\hbar/2m)\mathbf{q}^2+\Omega_l]t_n}e^{-i[(\hbar/2m)(\mathbf{q}+\mathbf{k})^2+\Omega_{l'}](t-t_n)}\\&\qquad+\sum_u e^{i\varphi}|u'\rangle\sum_{\mathbf{q}}C_{u\mathbf{q}}e^{i(\mathbf{q}-\mathbf{k})\cdot\mathbf{r}}e^{-i(\hbar/2m)(\mathbf{q}^2+\Omega_u)t_n}e^{-[(\hbar/2m)(\mathbf{q}-\mathbf{k})^2+\Omega_{u'}](t-t_n)}\Bigg]\,.\end{aligned}\tag{C24}$$

The three terms of (C24) proportional to 1, $\cos\theta$, and $i\sin\theta$ correspond to the three cases of (3.9). On the other hand, the decomposition into $\sum_\mu|\mu\rangle$, $\sum_l|l'\rangle$, $\sum_u|u'\rangle$ gives the three cases of (3.10); note the momenta $\mathbf{q}$, $\mathbf{q}+\mathbf{k}$, $\mathbf{q}-\mathbf{k}$ in the exponent.

We have assumed exact resonance, but any detuning ($\ll\tau^{-1}$) can be allowed for by replacing φ with $\varphi+(\omega+\Omega_l-\Omega_u)t_n$. Repeated application of (C24) then leads to formulas (3.8)–(3.19) and to Rules 1–3. If the atomic spectrum is more complicated, containing harmonic vibrational modes or hyperfine Raman transitions, or if more than one $\mathbf{k}$ is active simultaneously, the Hamiltonian needs to be treated in larger than 2×2 blocks and the simple expressions (3.9) are replaced by an array of transition amplitudes that may or may not be easy to calculate; but apart from this change the "Feynman" rules remain the same.

6. Standing-wave excitation

One generalization, that of a standing wave with $\mathbf{k}$ and $-\mathbf{k}$ simultaneously active and of equal strengths, is easily

treated. Since there is only one frequency present, the Hamiltonian is still resolved into 2×2 blocks. The field may be written spatially as proportional to

$$e^{i(\mathbf{k}\cdot\mathbf{r}-\omega t-\varphi^+)}+e^{i(-\mathbf{k}\cdot\mathbf{r}-\omega t-\varphi^-)}$$
$$=2e^{-i\omega t}e^{-i(\varphi^++\varphi^-)/2}\sin\left[\mathbf{k}\cdot\mathbf{r}-\frac{\varphi^+-\varphi^-}{2}+\frac{\pi}{2}\right].$$

Neglecting atomic motion during the pulse, we may say that an atom at $\mathbf{r}$ feels a pulse of area

$$\theta(\mathbf{r})=\theta_0\sin\left[\mathbf{k}\cdot\mathbf{r}-\frac{\varphi^+-\varphi^-+\pi}{2}\right],$$

where θ_0 is the area felt at the crest of the standing wave.

Using the formula

$$e^{i[\theta(\mathbf{r})/2]}=e^{(1/2)i\theta_0\sin(\mathbf{k}\cdot\mathbf{r}-\varphi)}$$
$$=\sum_{-\infty}^{+\infty}J_m\left[\frac{\theta_0}{2}\right]e^{im(\mathbf{k}\cdot\mathbf{r}-\varphi)},$$

where $\varphi=(\varphi^+-\varphi^-+\pi)/2$, we see that the even m contribute to $\cos[\frac{1}{2}\theta(\mathbf{r})]$ and the odd to $i\sin[\frac{1}{2}\theta(\mathbf{r})]$. The factor $e^{-i(\varphi^++\varphi^-)/2}$ determines the origin of the rotating coordinate system and therefore enters only into active transitions (odd m). The result is that in (C24) the product $(\cos\frac{1}{2}\theta)e^{i\mathbf{q}\cdot\mathbf{r}}$ should be replaced by

$$\sum_{m\ \text{even}}J_m(\tfrac{1}{2}\theta_0)e^{i(\mathbf{q}+m\mathbf{k})\cdot\mathbf{r}-m(\varphi^+-\varphi^-+\pi)/2},$$

and $(\sin\frac{1}{2}\theta)e^{i(\mathbf{q}\pm\mathbf{k})\cdot\mathbf{r}}$ should be replaced by

$$e^{\mp i(\varphi^++\varphi^-)/2}\sum_{m\ \text{odd}}J_m(\tfrac{1}{2}\theta_0)e^{i(\mathbf{q}+m\mathbf{k})\cdot\mathbf{r}-m(\varphi^+-\varphi^-+\pi)/2}.$$

This leads to Rules 1′ and 2′ as modified for standing waves in Sec. II F.

Note that for small θ_0 the phases and amplitudes of the terms in $m=0,\pm1$ reproduce the inactive and active transitions due to the separately considered traveling waves with wave vectors $+\mathbf{k}$ and $-\mathbf{k}$ and areas $\theta_0/2$.

[1] R. Beach, S. R. Hartmann, and R. Friedberg, Phys. Rev. A **25**, 2658 (1982).

[2] L. Allen and J. H. Eberly, *Optical Resonance and Two-Level Atoms* (Dover, New York, 1987)

[3] S. L. McCall and E.L. Hahn, Phys. Rev. Lett. **18**, 908 (1967).

[4] N. A. Kurnit, I. D. Abella, and S. R. Hartmann, Phys. Rev. Lett. **13**, 567 (1964).

[5] M. Kasevich and S. Chu, Phys. Rev. Lett. **67**, 181 (1991).

[6] F. Riehle, T. Kisters, A. Witte, J. Helmcke, and C. J. Bordé, Phys. Rev. Lett. **67**, 177 (1991).

[7] D. W. Keith, M. L. Schattenburg, H. I. Smith, and D. E. Pritchard, Phys. Rev. Lett. **61**, 1580 (1988).

[8] O. Carnal and J. Mlynek, Phys. Rev. Lett. **66**, 2689 (1991).

[9] J. J. Berkhout, O. J. Luiten, I. D. Setija, T. W. Hijmans, T. Mizusaki, and J. T. M. Walraven, Phys. Rev. Lett. **63**, 1689 (1989).

[10] P. L. Gould, G. A. Ruff, and D. E. Pritchard, Phys. Rev. Lett. **56**, 827 (1986).

[11] N. F. Ramsey, Phys. Rev. **78**, 695 (1950).

[12] T. W. Mossberg, R. Kachru, E. Whittaker, and S. R. Hartmann, Phys. Rev. Lett. **43**, 851 (1979).

[13] R. Beach, B. Brody, and S. R. Hartmann, Phys. Rev. A **27**, 2537 (1983).

[14] R. Beach, B. Brody, and S. R. Hartmann, Phys. Rev. A **27**, 2925 (1983).

[15] V. P. Chebotayev, in *Coherent Nonlinear Optics*, edited by M. S. Feld and V. S. Letokov, Topics in Current Physics Vol. **21** (Springer-Verlag, Berlin, 1980), pp. 59–109.

[16] This "area" has nothing to do with the "pulse area" θ which measures the strength of the laser excitation pulse.

[17] For illustration we note that for two-level atoms initially in the ground state, we have, just before the first pulse at t_1,

$$\Psi(\mathbf{r}_1,\ldots,\mathbf{r}_N,t_{1-})=\prod_s[|\mathrm{gr}\rangle_s\psi_{s0}(\mathbf{r}_s-\mathbf{R}_s)]$$

and this is converted by a pulse of area θ and phase φ into

$$\Psi(\mathbf{r}_1,\ldots,\mathbf{r}_N,t_{1-})=\prod_s[(|\mathrm{gr}\rangle_s\cos\tfrac{1}{2}\theta+ie^{i\mathbf{k}\cdot\mathbf{r}_s-i\varphi}|\mathrm{ex}\rangle_s\sin\tfrac{1}{2}\theta)\psi_{s0}(\mathbf{r}_s-\mathbf{R}_s)].$$

Apart from the factor $e^{i\mathbf{k}\cdot\mathbf{r}_s}$, this expression recalls the ordinary small-sample Bloch state

$$\prod_s\begin{bmatrix}\cos\frac{1}{2}\theta\\ i\sin\frac{1}{2}\theta\exp(-i\varphi)\end{bmatrix}$$
$$=\exp\left[i\theta\sum_s(S_x\cos\varphi-S_y\sin\varphi)\right]\prod_s\begin{bmatrix}1\\0\end{bmatrix},$$

where $|\mathrm{gr}\rangle=\binom{1}{0}$, $|\mathrm{ex}\rangle=\binom{0}{1}$, $S_x=\frac{1}{2}\left(\begin{smallmatrix}0&1\\1&0\end{smallmatrix}\right)$, $S_y=\frac{1}{2}\left(\begin{smallmatrix}0&-i\\i&0\end{smallmatrix}\right)$. This state can be expressed in Dicke's [18] basis as $\sum_m C_m|r=N/2,m\rangle$, where

$$C_m=\begin{bmatrix}N\\ \frac{1}{2}N+m\end{bmatrix}\cos^{(1/2)N+m}\theta\sin^{(1/2)N+m}$$
$$\times\theta\exp[i(\tfrac{1}{2}N-m)(\pi/2-\varphi)],$$

but it should not be confused with a single Dicke state $|r,m\rangle$, in which the excitation number $\frac{1}{2}N-m$ is known and the phase φ is completely indeterminate.

[18] R. H. Dicke, Phys. Rev. **93**, 99 (1954).

[19] A more explicit derivation would start with the density matrix as

$$\rho=\prod_s\int d^3\mathbf{r}\int d^3\mathbf{r}'|\mathbf{r}\rangle_s\Psi_s(\mathbf{r})\Psi_s^\dagger(\mathbf{r}')_s\langle\mathbf{r}'|$$

and the operator $\mathbf{T}_\mathbf{k}$ as

$$\mathbf{T}_\mathbf{k}=\mathbf{p}\sum_s |\mathrm{gr}\rangle_s \left[\int d^3\mathbf{r}|\mathbf{r}\rangle_s e^{-i\mathbf{k}\cdot\mathbf{r}}{}_s\langle\mathbf{r}|\right]_s \langle \mathrm{ex}| \prod_{s'(\neq s)} \mathbb{1}_{s'} .$$

Proceeding this way is more cumbersome but it brings out the point that we are really dealing with N-atom operators. Since these operators act only on one atom at a time and they are acting on product states, the formulas boil down to single-atom wave functions as presented in the text.

[20] The neglect of H_{kin} during τ is equivalent to supposing that the pulse is so short that is resonates with the whole Doppler-broadened line. This was not so in the gravity experiment [2], but by setting $\omega_m \cong G\tau k$ in that experiment they achieved the same effect as though the pulses were short.

[21] R. Friedberg and S. R. Hartmann, Laser Phys. **3**, 526 (1993).

[22] R. Friedberg and S. R. Hartmann, Laser Phys. (to be published).